

TOPICAL REVIEW • OPEN ACCESS

Genetically encodable fluorescent protein markers in advanced optical imaging

To cite this article: Karin Nienhaus and Gerd Ulrich Nienhaus 2022 *Methods Appl. Fluoresc.* **10** 042002

View the [article online](#) for updates and enhancements.

You may also like

- [Synthesis, properties and self-organization of meso-arylporphyrins with higher alkyl substituents](#)

Natal'ya A. Bragina, Kseniya A. Zhdanova and Andrey F. Mironov

- [Hybrid materials based on graphene derivatives and porphyrin metal-organic frameworks](#)

Vladimir V. Arslanov, Maria A. Kalinina, Elizaveta V. Ermakova et al.

- [Porous porphyrin-based metal-organic frameworks: synthesis, structure, sorption properties and application prospects](#)

Yulia G. Gorbunova, Yulia Yu. Enakieva, Marina V. Volostnykh et al.



**NOW WITH MICROPL UPGRADE
FOR SPECTRAL AND TIME-RESOLVED
PHOTOLUMINESCENCE MICROSCOPY.**



edinst.com

Methods and Applications in Fluorescence



TOPICAL REVIEW

Genetically encodable fluorescent protein markers in advanced optical imaging

OPEN ACCESS

RECEIVED

21 March 2022

REVISED

1 June 2022

ACCEPTED FOR PUBLICATION

29 June 2022

PUBLISHED

28 July 2022

Original content from this work may be used under the terms of the [Creative Commons Attribution 4.0 licence](#).

Any further distribution of this work must maintain attribution to the author(s) and the title of the work, journal citation and DOI.



Karin Nienhaus¹ and Gerd Ulrich Nienhaus^{1,2,3,4,*}

¹ Institute of Applied Physics, Karlsruhe Institute of Technology, 76049 Karlsruhe, Germany

² Institute of Nanotechnology, Karlsruhe Institute of Technology, 76021 Karlsruhe, Germany

³ Institute of Biological and Chemical Systems, Karlsruhe Institute of Technology, 76021 Karlsruhe, Germany

⁴ Department of Physics, University of Illinois at Urbana–Champaign, Urbana, IL 61801, United States of America

* Author to whom any correspondence should be addressed.

E-mail: uli@uiuc.edu

Keywords: fluorescence microscopy, super resolution microscopy, genetically encodable fluorescent markers, GFP-type fluorescent protein, tetrapyrrole-binding fluorescent protein

Abstract

Optical fluorescence microscopy plays a pivotal role in the exploration of biological structure and dynamics, especially on live specimens. Progress in the field relies, on the one hand, on technical advances in imaging and data processing and, on the other hand, on progress in fluorescent marker technologies. Among these, genetically encodable fluorescent proteins (FPs) are invaluable tools, as they allow facile labeling of live cells, tissues or organisms, as these produce the FP markers all by themselves after introduction of a suitable gene. Here we cover FP markers from the GFP family of proteins as well as tetrapyrrole-binding proteins, which further complement the FP toolbox in important ways. A broad range of FP variants have been endowed, by using protein engineering, with photophysical properties that are essential for specific fluorescence microscopy techniques, notably those offering nanoscale image resolution. We briefly introduce various advanced imaging methods and show how they utilize the distinct properties of the FP markers in exciting imaging applications, with the aim to guide researchers toward the design of powerful imaging experiments that are optimally suited to address their biological questions.

1. Introduction

Over the past decades, optical fluorescence microscopy has taken center stage as a technique for studying biomolecular structure, dynamics and interactions, as well as the resulting functional consequences within living cells, tissues, or organisms, as they occur in space and time. It is a highly sensitive and minimally invasive technique, allowing experiments to be performed over extended periods on live specimens under near-physiological conditions.

The enormous power and versatility of present-day optical fluorescence microscopy rests on two pillars. On the one hand, powerful microscopy hardware has become available that allows imaging with high temporal and spatial resolution and excellent signal-to-background ratio (SBR) [1, 2]. Various super-resolution methods have been devised that permit routine optical fluorescence imaging with 10–100 nm

resolution [3–5]. On the other hand, equally important has been the invention of ingenious procedures to decorate—with molecular precision and specificity—locations within a sample with luminescent probes. A variety of strategies have become available to precisely tag biological molecules or structures with fluorophores, so they can be visualized selectively in the presence of a myriad of other molecules. In general, fluorescence labeling can require enormous efforts and potentially affect the molecular processes under study and their biological effects [6–8]. A huge simplification was achieved by the introduction of genetically encodable fluorescence tags. By introducing a suitably engineered gene, e.g., a fusion construct of a protein with such a tag, into cells, we enable the biological system (cell, tissue, or organism) to produce the tagged protein autonomously; often cumbersome staining procedures are no longer needed. Genetically encodable fluorescence tags greatly facilitate specific

labeling and enable entirely new experiments. For truly self-luminescent tags such as GFP-type markers, the protein lights up after expression and can be visualized [9–11]. For tetrapyrrole-binding tags (section 3), chemical tags (e.g., Halo, SNAP/CLIP) [12–14] and RNA aptamer tags [15–17], specifically binding chromophores need to be supplied externally or internally via metabolic processes.

In this review, we summarize the current state of genetically encoded fluorescent protein markers, including green fluorescent protein (GFP)-type proteins and tetrapyrrole-binding fluorescent proteins (FPs). GFP-type markers comprise a huge family of proteins with diverse photophysical properties, making them extremely versatile. Nevertheless, there are limitations inherent in their design that cannot be overcome by protein engineering. They require dioxygen (and produce hydrogen peroxide) in the chromophore maturation process and, therefore, are not suited for imaging in anaerobic environments such as bacterial biofilms and tumor cores. Moreover, although their wavelength range has been extended towards the red over the years, far-red (650–700 nm) GFP-type markers lack brightness, and emission in the near-infrared (NIR, 700–1000 nm) region does not appear to be feasible. These long-wavelength spectral regions are particularly attractive for deep-tissue and whole-animal imaging, however, due to lower light scattering and absorption in biological tissues. Tetrapyrrole-binding FPs function in anaerobic environments and emit long-wavelength fluorescence, so they can nicely complement or substitute GFP-type markers in a variety of imaging applications.

Many of these genetically encodable markers feature very special physico-chemical properties that make them suitable for particular fluorescence imaging techniques (and less suitable for others). Thus, it is crucially important to select a fluorescence marker that best supports the selected imaging mode, a ‘one-dye-fits-all’ approach will not be successful. Therefore, we briefly introduce these methods, discuss suitable FP markers and illustrate their use with selected applications.

2. GFP-type fluorescent proteins

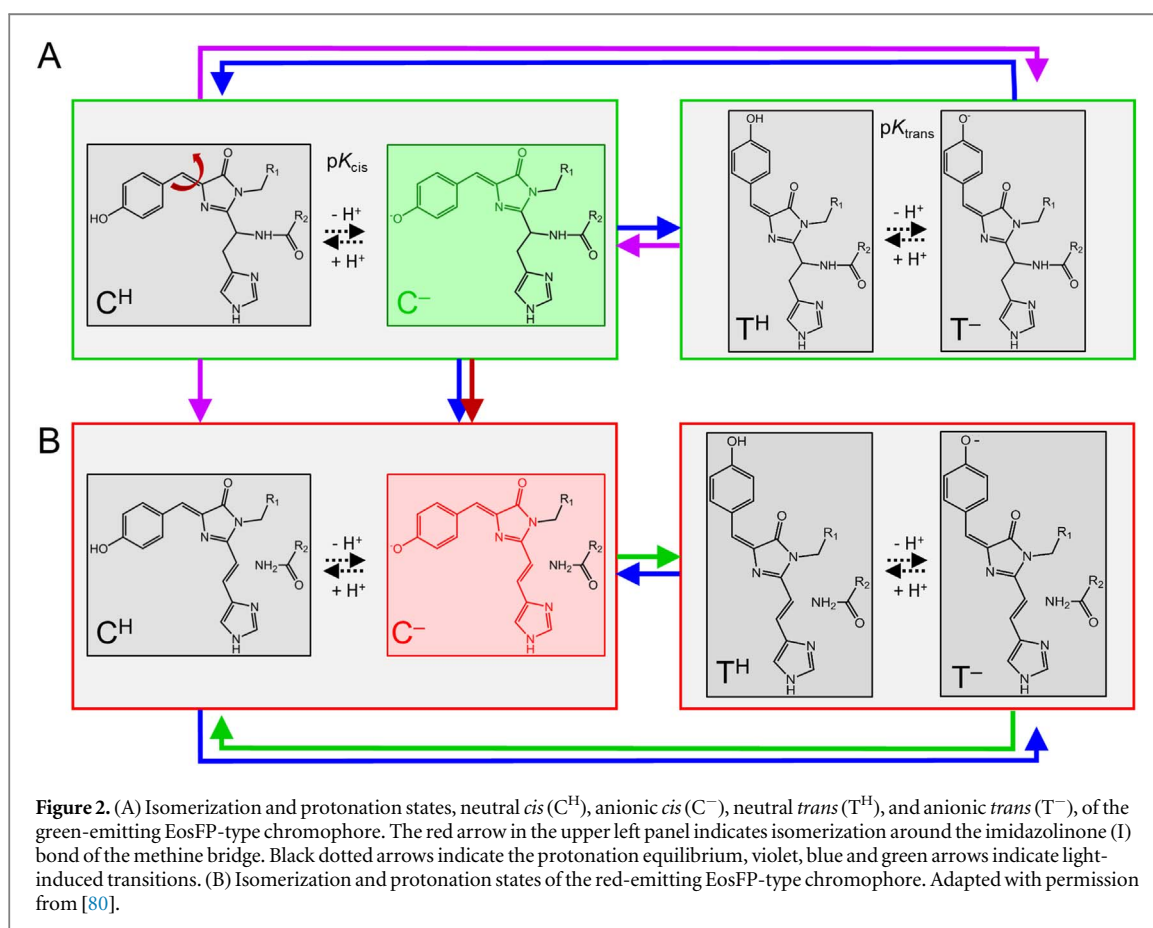
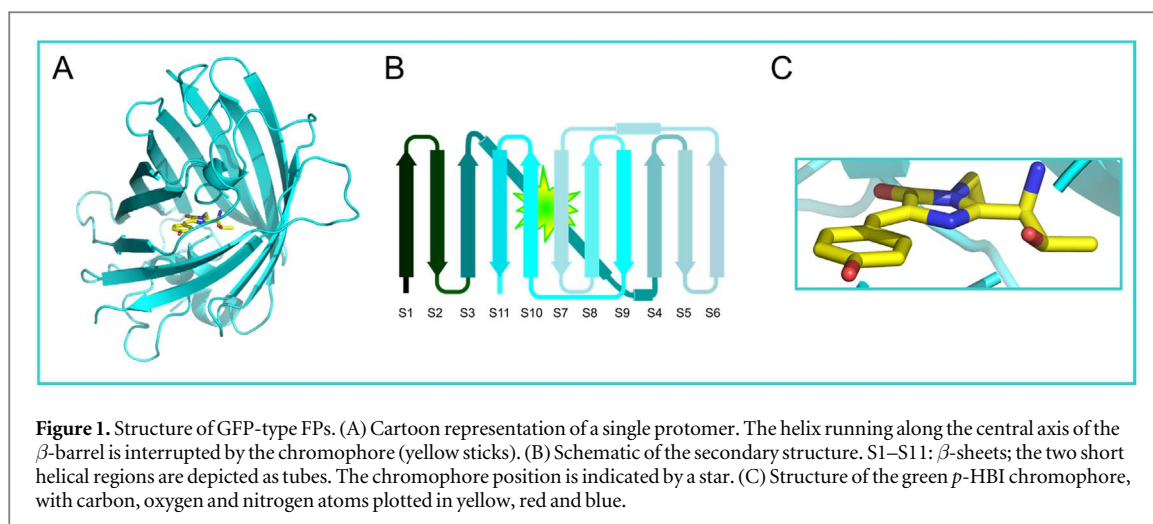
2.1. Basic photochemical and optical properties

The green fluorescent protein (GFP) and related fluorescent proteins (FPs) of the GFP family have revolutionized research in the life sciences by enabling a vast array of novel fluorescence-based approaches to study biomolecular processes, especially in living cells and organisms [18, 19]. Osamu Shimomura isolated GFP from tissue extracts of the jellyfish *Aequorea victoria* already in 1962 [20]. But only in 1994, researchers recognized the usefulness of avGFP as a genetically encoded fluorescence marker, just requiring (usually prevalent) O₂ for its self-assembly, which is necessary for fluorophore synthesis from a

tripeptide [9, 10, 21]. Color variants of avGFP with emission peaks ranging from blue (BFP) to yellow (YFP) were quickly developed by mutagenesis [22]. A major advance was the discovery of GFP homologues in anthozoa animals [23, 24], complementing the color palette with orange and red FP markers [25, 26]. Furthermore, it was realized that certain FPs undergo a variety of light-induced chromophore modifications, making their fluorescence controllable by light [27–30]. Upon irradiation with light of a suitable wavelength, ‘photoactivatable’ or ‘optical highlighter’ FPs either switch reversibly between a fluorescent and a non-fluorescent state (photoswitching), or change their fluorescence emission intensity or color irreversibly (photoconversion).

All FPs of the GFP family fold into a rigid, 11-stranded β -can, with a central helix running along its axis, capped at either end by short helical sections and loops (figures 1(A), (B)). The fluorescent chromophore interrupts the central helix and resides close to the geometrical center of the protein. The green-emitting 4-(*p*-hydroxybenzylidene)–5-imidazolinone (*p*-HBI) chromophore (figure 1(C)) forms autocatalytically from three amino acids (Ser65–Tyr66–Gly67, GFP numbering) in a sequential cyclization-oxidation-dehydration reaction, with characteristic time scales ranging from minutes to hours [31, 32]. There are two isomeric forms of *p*-HBI (figure 2(A)), with the *cis* isomer being thermodynamically more stable than the *trans* isomer for the free dye in aqueous solution [33]. The *p*-HBI molecule is completely non-fluorescent in solution because it effectively de-excites non-radiatively upon rotation around one of the bonds of the methine bridge, thanks to a low isomerization barrier [34–36]. Thus, a rigid binding pocket, with surrounding residues and water molecules stabilizing the planar conformation within the β -can, is essential to ensure a high quantum yield (QY) of fluorescence emission. Most natural GFP-type proteins characterized to date host a fluorescent *cis* chromophore, with the red-emitting eqFP611 [37] being a notable exception [38]. Likewise, among engineered FPs, a fluorescent anionic *trans* chromophore is rarely observed [39–41].

In either isomeric state, the hydroxyphenyl moiety of the chromophore can, in principle, be protonated or deprotonated (figure 2(A)). Typically, only the anionic form is strongly fluorescent; the neutral chromophore emits only weakly (if at all), or is rendered anionic upon photoexcitation and excited-state proton transfer (ESPT, see section 2.2.1). In optical absorption spectra, the neutral and anionic chromophore species display two bands (ca. 390 and 490 nm for green-emitting FPs), denoted A and B, respectively [42, 43]. The pH-dependent change of the A and B band amplitudes often cannot be described by a simple protonation reaction according to the Hendersson-Hasselbalch relation [44–46]. Chromophore protonation is coupled to the external proton concentration; nevertheless, tight electrostatic interactions between



the chromophore and protonatable groups in the protein interior can cause anomalous behavior such as constant A and B band populations in a certain pH range [44, 47] or multiple protonation steps [48, 49]. Comparing *cis* and *trans* isomers, the A band peak positions are only slightly different, and the same holds true for the B bands. Thus, the isomeric state cannot easily be assigned from the absorption spectra [38, 49, 50].

Natural FP polypeptide sequences are generally poor performers as FP markers and need further

optimization by protein engineering. Four main issues require particular attention. (1) Natural polypeptide chains frequently tend to aggregate or oligomerize, which is detrimental for their use as a fusion marker tied to a protein of interest [32, 51, 52]. In lucky cases, monomeric markers have been obtained by exchanging only a few amino acids at the binding interfaces [40, 41, 53, 54], but oftentimes, dozens of replacements are required [40, 55, 56]. (2) FPs display incomplete or, in rare cases, even complete lack of chromophore formation (maturation) [32, 52, 57],

Table 1. Optical properties of selected bright GFP-type FPs across a wide wavelength range.

FP	λ_{Exc} (nm)	λ_{Em} (nm)	ϵ ($M^{-1}cm^{-1}$)	QY	Brightness ^a	References
Sirius	355	424	15,000	0.24	3.6	[253]
mTagBFP2	399	454	50,600	0.64	32.38	[254]
mCerulean3	433	475	40,000	0.87	34.8	[255]
mEGFP	488	507	56,000	0.6	33.6	[53]
mNeonGreen	506	517	116,000	0.8	92.8	[256]
mClover3	506	518	109,000	0.78	85.02	[257]
mVenus	515	527	104,000	0.64	66.56	[258]
mRuby	558	605	112,000	0.35	39.2	[40]
mScarlet	569	594	100,000	0.7	70	[71]
mCherry	587	610	72,000	0.22	15.84	[259]
mGarnet2	598	671	105,000	0.09	9.13	[151]
mCardinal	604	659	87,000	0.19	16.53	[260]

^a defined as $(\epsilon \times QY)/1000$.

especially upon expression at ‘higher’ temperatures (37 °C) [58]. In many cases, researchers have succeeded in introducing amino acid modifications that yielded optimized maturation [39, 53, 59]. (3) The resistance against irreversible photobleaching of *p*-HBI and its variants is generally weaker in comparison to robust synthetic dyes. Enhancing the thermodynamic stability and rigidity of the FP fold to suppress chromophore mobility may help to enhance photobleaching resistance. (4) FPs are by no means steady light emitters but show intermittent fluorescence (photodynamics, flickering) on timescales ranging from nanoseconds to minutes, as observed early on by Moerner and collaborators [60]. There are various reversible processes that the chromophore can undergo to switch between dark and bright (emitting) states, including formation of triplet or radical states [61–63], proton transfer and/or conformational dynamics such as *cis*–*trans* isomerization [64–66], and transient photoinduced electron transfer, i.e., photooxidation or photoreduction [67–70].

Over several decades, a wealth of detailed structural and spectroscopic studies have paved the way to a profound understanding of structure-function relationships of GFP-like proteins, providing a basis for the rational development of optimized variants by using genetic engineering [18]. Rational amino acid modifications are typically complemented by random mutagenesis steps, which sometimes introduce rather unexpected but effective modifications that are not always easy to rationalize. Rather than starting marker development from a single template structure, one can also synthesize the FP from multiple short stretches of amino acids taken from FPs with beneficial properties, as exemplified with mScarlet [71].

For a live bioimaging experiment, FP markers must be chosen with a view toward the micro-environment(s) in which they need to function. For example, FPs targeting the endosomal pathway will encounter pH values ranging from 6.5 (in early

endosomes) to 4.5 (in lysosomes). Unless the chromophore $pK < 4$, the decrease of pH makes the sample dimmer due to a serious reduction of the fraction of anionic, fluorescent chromophores. Moreover, oxidizing micro-environments such as the eukaryotic secretory pathway and the mitochondrial inner membrane space promote disulfide bond formation. Accordingly, cysteines in the FP polypeptide chain can cause problems and lead to non-functional marker constructs [72]. This problem has been solved by the development of various ‘oxFPs’ that have their cysteines replaced, e.g., moxNeonGreen [73]. Another potential problem is the generation of reactive oxygen species (ROS) upon FP marker excitation in an oxidative environment, leading to phototoxicity especially under prolonged imaging conditions [74]. In many applications, the effect is negligible because the β -can effectively screens the chromophore from O_2 . In the engineered FP KillerRed [75] and its monomeric variant SuperNova [76], diffusion of O_2 towards the chromophore has been facilitated by a water-filled channel so that these FPs are orders of magnitude more phototoxic than avGFP and can be used as genetically encoded photosensitizers.

A small selection of monomeric FPs with high molecular brightness, i.e., extinction coefficient, ϵ , times QY, covering a major range of the visible spectrum, are given in table 1. A comprehensive list of FP marker tools can be found in the FP database together with key optical properties [77]. Presently, the FP database contains more than 800 entries, ca. 200 of which are monomeric FPs. Even though determination of photophysical parameters such as ϵ and QY are simple procedures, literature values should generally not be taken at face value. For example, an early literature survey found ϵ values ranging from 6,000–50,000 $M^{-1}cm^{-1}$ for the B band of avGFP [47], and ϵ values of 27,000 [78] and 97,000 $M^{-1}cm^{-1}$ [79] have been reported for the green chromophore species of mEosFP*thermo*.

Table 2. Optical properties of selected (reversibly) photoswitchable GFP-type FPs (PS-FPs).

Parental FP	Name	λ_{Exc} (nm)	λ_{Em} (nm)	ϵ ($M^{-1}cm^{-1}$)	QY	Brightness ^a	References
Dronpa	Dronpa	503	518	95,000	0.85	80.75	[224]
	ffDronpa	503	517	105,000	0.75	78.75	[261]
	Padron	503	522	43,000	0.64	27.52	[262]
	Kohinoor	495	514	62,900	0.71	44.66	[263]
mEos2	mGeos-F	504	515	53,135	0.85	45.16	[162]
	mGeos-S	501	512	64,602	0.76	49.1	[162]
	mGeos-E	501	513	69,630	0.75	52.22	[162]
	mGeos-C	505	516	76,967	0.81	62.34	[162]
mEos3.1	Skylan-NS	499	511	133,770	0.59	78.92	[184]
	Skylan-S	499	511	152,408	0.64	97.54	[223]
mMaple3	G-Mars Q	470	494	38,615	0.64	24.71	[169]
	G-Mars L	468	495	43,278	0.50	21.64	[168]
avGFP	rsEGFP	493	510	47,000	0.36	16.92	[264]
	rsEGFP2	478	503	61,300	0.3	18.39	[164]
	Dreiklang	511	529	83,000	0.41	34.03	[89]
	SPOON	510	527	54,000	0.5	27	[90]
DsRed	rsCherryRev	572	608	84,000	0.005	0.42	[92]
	rsCherry	572	610	80,000	0.02	1.6	[92]
TagRFP	rsFusionRed1	577	605	82,400	0.1	8.24	[173]
	rsTagRFP	567	585	36,800	0.11	4.05	[265]

^a defined as $(\epsilon \times QY)/1000$.

2.2. Chromophore photophysics

In GFP-type proteins, the chromophore shows surprising photochemical and photophysical effects that can be both a blessing and a curse [80, 81]. For example, they universally display intermittent fluorescence emission, which can be detrimental when a bright and steadily emitting fluorophore is needed, e.g., for single particle tracking, but is essential in super-resolution imaging applications [82]. We briefly introduce different classes of light-responsive FPs in the following subsections.

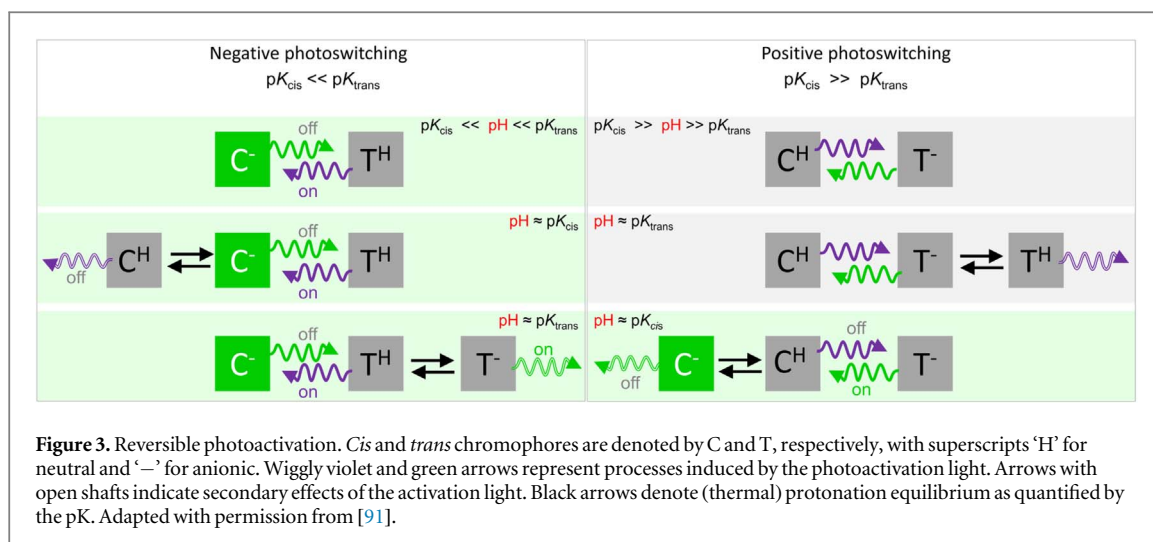
2.2.1. Large Stokes-shift (LSS) FPs exploiting excited-state proton transfer (ESPT)

In avGFP, B band excitation (~ 488 nm) of the anionic chromophore gives rise to fluorescence peaking at 504 nm [83]. Remarkably, A band excitation (~ 400 nm) of the neutral chromophore yields a similar emission peak (~ 508 nm) and thus a Stokes shift of more than 100 nm due to ESPT [35, 43]. The hydroxyphenyl group of the *p*-HBI chromophore is a photoacid that can release its proton upon electronic excitation to a nearby proton acceptor, from where it returns once the chromophore's electronic system has relaxed to the ground state [43, 84]. In recent years, ESPT pathways have been engineered into various red-emitting FPs to generate LSS variants [85–87]. Their neutral chromophores can be excited with 473- or 488-nm laser lines and emit fluorescence at or above 600 nm. Thus, in combination with a regular green-emitting FP, dual-color experiments can be performed with only one excitation laser [87, 88].

2.2.2. Photoswitchable FPs

Reversibly photoactivatable, or photoswitchable FPs (PS-FPs, see table 2) can be toggled between a dark off- and a bright on-state by light. In all known PS-FPs (except for Dreiklang [89] and SPOON [90], see below), photoswitching involves a light-induced, strictly correlated change of the isomerization and protonation states of the chromophore, accompanied by conformational rearrangements of amino acids lining the chromophore pocket [91]. The proton affinity of the chromophore's hydroxyphenyl moiety, as quantified by its *pK* value, plays a pivotal role in the switching process. In general, the *pK* is different for the *cis* and *trans* forms due to the different local environments of the protonating group. Altogether, there are four distinct chromophore species involved in photoswitching, the anionic *cis* chromophore, C^- , which is the key fluorescent species in most PS-FPs, the anionic *trans* chromophore, T^- , and the neutral *cis* and *trans* chromophores, C^H and T^H (figure 2(A)).

In so-called negative photoswitchers [92], the proton binding affinity is lower for the *cis* than the *trans* isomer and, thus, $pK_{cis} < pK_{trans}$. If the sample pH is in-between, i.e., $pK_{cis} < pH_{sample} < pK_{trans}$, only two fluorophore species, C^- and T^H , will be populated appreciably in equilibrium (figure 3(A)). Excitation into the B band of the fluorescent C^- state (with ~ 480 nm light for green PS-FPs) induces emission and, with low probability, a transition to the non-fluorescent T^H form (off-switching). Irradiating into the A band of the non-fluorescent T^H form (~ 400 nm for green-emitting PS-FPs) induces the reverse transition and, therefore, restores the fluorescent C^- state (on-switching). At lower sample pH, i.e.,



$pK_{cis} \approx pH_{sample} < pK_{trans}$, C^H becomes populated appreciably. Again, exciting C^- results in emission and, with a small probability, induces a transition to the dark T^H form. 400-nm light, however, excites both T^H and C^H , so that *trans-cis* and *cis-trans* isomerization reactions are simultaneously photoactivated. The net result is a reduced fraction of the C^- species; on-switching is incomplete. Similarly, at higher sample pH, $pK_{cis} < pH_{sample} \approx pK_{trans}$, the fraction of T^- species becomes significant and gives rise to more complicated behavior.

The acid-tolerant PS-FPs rsGamillus-S and rsGamillus-F, engineered from Gamillus, a monomeric green FP from the hydromedusa *Olindias formosus*, are as yet the only known negative photoswitchers having T^- as the fluorescent state [93]. Here, the roles of *cis* and *trans* chromophores are exchanged; these PS-FPs can be switched off by exciting T^- with ~500 nm light, and switched on by exciting C^H with ~400 nm light.

For so-called positive photoswitchers [92], $pK_{cis} > pK_{trans}$; excitation within the spectral region of the B band enhances the emission, but only if the sample pH is such that $pK_{cis} \approx pH > pK_{trans}$. This condition means that the *trans* isomer is mainly deprotonated, whereas the *cis* isomer is a mixture of neutral and anionic species. For on-switching, excitation light (~480 nm light for green-emitting PS-FPs) is absorbed by the B band of the T^- species, which leads to its photoisomerization and thus enhances C^H (figure 3(B)). Subsequently, C^H transfers population to C^- to restore the protonation equilibrium, so that the fraction of the fluorescent species, C^- , is enhanced. Because the B bands of T^- and C^- overlap strongly, the newly generated C^- species will also be photoactivated to undergo *cis-trans* isomerization, which reduces its population. The net effect of irradiation into the B band region depends on the relative populations of both anionic forms and their associated photoisomerization QYs. The off-transition is induced by excitation of the A band of the C^H species (~400 nm for green-emitting PS-FPs), which

photoisomerizes to form non-fluorescent T^- . Subsequently, the protonation equilibrium between C^H and C^- re-adjusts, causing a reduction of the fluorescent C^- species. For higher sample pH, $pK_{cis} > pH_{sample} > pK_{trans}$ or $pK_{cis} > pH \approx pK_{trans}$, there is no change in fluorescence upon light-activated isomerization.

Reversible on- and off switching in Dreiklang requires illumination wavelengths of ~365 nm and ~405 nm, respectively [89]. Fluorescence excitation at ~515 nm is completely decoupled from photoswitching and leads to emission peaking at 529 nm. In the on-state, the chromophore exists in both protonated and deprotonated forms, with the A and B absorption bands centered on 412 and 511 nm, respectively. Irradiation into the B band induces fluorescence, whereas irradiation into the A band leads to a remarkable covalent hydration of the imidazolinone ring, resulting in a non-fluorescent chromophore absorbing at 340 nm. Subsequent irradiation into this band dissociates the water molecule again to recover the on-state chromophore. Water binding is weak, so on-switching can also occur thermally. A Dreiklang variant, SPOON [90], can be switched off by 488-nm excitation light and rekindles via thermally induced dehydration.

2.2.3. Irreversible photoconversion of the FP chromophore

In photoconverting FPs, the chromophore is irreversibly altered by light exposure. Van Thor *et al* [94] reported in 2001 that intense illumination of avGFP with 390-nm light did not only result in green fluorescence, but also increased the fraction of anionic chromophore species. They showed that photoconversion involves a one-photon process causing CO_2 cleavage from Glu222. The Thr203His variant of avGFP, denoted photoactivatable GFP (PA-GFP), is initially stabilized in the neutral *cis* form of the chromophore and, therefore, essentially non-emissive upon excitation at 488 nm [95]. Excitation into the A band results in green emission due to ESPT, as in avGFP. Decarboxylation of the Glu222 side chain

Table 3. Optical properties of off-on photoconvertible GFP-type FPs.

FP	λ_{Exc} (nm)	λ_{Em} (nm)	ϵ ($M^{-1} cm^{-1}$)	QY	Brightness ^a	References
PA-GFP	504	517	17,400	0.79	13.75	[95]
PATagRFP	562	595	66,000	0.38	25.08	[266]
PAmCherry1	564	595	18,000	0.46	8.28	[267]
PAmCherry2	570	596	24,000	0.53	12.72	[267]
PAmCherry3	570	596	21,000	0.24	5.04	[267]
PAmKate	586	628	25,000	0.18	4.5	[268]

^a defined as $(\epsilon \times QY)/1000$.

Table 4. Optical properties of (irreversibly) photoconverting GFP-type FPs featuring a wavelength change, as indicated by the color bars.

FP	λ_{Exc} (nm)	λ_{Em} (nm)	ϵ ($M^{-1} cm^{-1}$)	QY	Bright-ness	λ_{Exc} (nm)	λ_{Em} (nm)	ϵ ($M^{-1} cm^{-1}$)	QY	Bright-ness	Ref.
mClavGR2	488	504	19,000	0.77	14.63	566	583	32,000	0.53	16.96	[269]
mKikGR	505	515	49,000	0.69	33.81	580	591	28,000	0.63	17.64	[56]
Dendra2	490	507	45,000	0.5	22.5	553	573	35,000	0.55	19.25	[97]
moxDendra2	490	504	50,300	0.5	25.15	551	571	31,200	0.55	17.16	[270]
NijiFP (rs)	469	507	41,100	0.64	26.3	526	569	42,000	0.65	27.3	[79]
mMaple	489	505	15,000	0.74	11.1	566	583	30,000	0.56	16.8	[271]
mMaple3	491	506	15,760	0.37	5.83	568	583	23,970	0.52	12.46	[199]
moxMaple3	490	506	14,800	0.37	5.48	569	584	24,230	0.52	12.6	[272]
mEos2-A69T	495	509	24,300	0.63	15.31	565	580	11,500	0.66	7.59	[273]
mEos3.1	505	513	88,400	0.83	73.37	570	580	33,500	0.62	20.77	[78]
mEos3.2	507	516	63,400	0.84	53.26	572	580	32,200	0.55	17.71	[78]
mEos4a	505	515	83,530	0.86	71.84	571	580	61,000	0.71	43.31	[238]
mEos4b	505	516	78,170	0.84	65.66	570	580	55,500	0.71	39.41	[238]
mEosFP	505	516	67,200	0.64	43.01	569	581	37,000	0.62	22.94	[54]
mEosFP $_{thermo}$	504	514	97,200	0.84	81.65	567	579	41,300	0.65	26.85	[104]
mIrisFP (rs)	486	516	47,000	0.54	25.38	546	578	33,000	0.59	19.47	[104]
PS-CFP	402	468	34,000	0.16	5.44	490	511	27,000	0.19	5.13	[274]
PS-CFP2	400	468	43,000	0.2	8.6	490	511	47,000	0.23	10.81	[275]
PSmOrange	548	565	113,300	0.51	57.78	634	662	32,700	0.28	9.16	[276]
PSmOrange2	546	561	51,000	0.61	31.11	619	651	18,900	0.38	7.18	[277]

upon intense violet (~ 400 nm) light irradiation causes a shift of the protonation equilibrium of the chromophore from the neutral to the bright green-fluorescent anionic form, and the emission intensity upon B band excitation increases ~ 100 -fold [96]. Various FPs of the PA-GFP type are listed in table 3.

Green-to-red photoconvertible FPs (PC-FPs) such as EosFP make up the largest family of photoconvertible FPs (table 4). A key advantage over PA-FPs is that they can easily be detected in the inactive, green-emitting state forming upon protein expression. With a low probability, excitation of the green form causes cleavage of the polypeptide chain between the $N\alpha$ and $C\alpha$ atoms of residue 62 of the chromophore tripeptide, His62-Tyr63-Gly64 (EosFP numbering [54]). The photoconversion reaction can be initiated most

effectively with light around 400 nm, i.e., by excitation of the neutral *cis* chromophore, and also via excitation of the anionic (green) chromophore (e.g., 488 nm) [97–99], albeit with very low yield (see also figure 5(A) in [54]). As a result, the conjugated π -electron system of the *p*-HBI chromophore extends to include the imidazole sidechain of His62 (figure 2(B)), causing a red shift of the absorption and emission bands. The two chain fragments remain tightly associated after photo-cleavage, preserving the proper β -can fold. Remarkably, exposure to far-red light (600–850 nm) in combination with 488-nm excitation light has been shown to greatly enhance the photoconversion yield in EosFP-type PC-FPs with Ala69Thr or Ala69Ser mutations [100–103]. This process, dubbed ‘primed conversion’, enables, e.g., dual-channel super-resolution

single-molecule localization microscopy (SMLM, see section 4.5) of primable EosFP variants together with the regular versions [101].

By introducing a single mutation (Phe173Ser) that gives the chromophore more space to move, PC-FPs have been engineered that, in addition to green-to-red photoconversion, also feature *cis-trans* isomerization-based photoswitching in the green and red forms. These variants, e.g., IrisFP [103], mIrisFP [104] and NijiFP [79] (table 4), can be employed, e.g., in super-resolved pulse-chase imaging experiments based on SMLM.

3. Linear tetrapyrrole-binding fluorescent proteins

In their quest for alternative platforms for engineering genetically encoded FP markers, researchers have identified various proteins that bind linear tetrapyrroles (e.g., bilirubin (BR), biliverdin IX α (BV), phycocyanobilin (PCB), phytychromobilin (P Φ B)), either non-covalently or covalently and autocatalytically, so that no further enzyme or cofactor is needed to generate a functional FP marker [105]. Like *p*-HBI derivatives in GFP-type FPs, linear tetrapyrroles are intrinsically flexible, and effective radiationless de-excitation due to fast intramolecular rotations makes them practically non-fluorescent in solution [106, 107]. Upon binding to a protein, however, they acquire a substantial fluorescence QY due to steric restrictions imposed by the protein. BR-binding markers fluoresce brightly in the green spectral range, whereas BV-binding marker proteins emit fluorescence in the far-red/NIR spectral regions. In contrast to GFP-type markers, which generate their chromophore autocatalytically, BR- and BV-binding proteins depend on an external supply of cofactors to form a functional FP marker. Both molecules are intermediates of the catabolism of heme, which is a key protein cofactor that is produced in significant amounts in various live animals, including fish and mammals. Notably, the performance of these fluorescence turn-on probes depends on the *in-situ* fractional occupation of their ligand binding sites and, therefore, on the ligand concentration in their environment (test tube, cell culture, organism etc) as well as the intrinsic ligand affinity of the marker protein. Accordingly, the excellent brightness under *in-vitro* conditions may not be reproduced in experiments with live animals, since limited bioavailability can severely hamper their performance [108].

3.1. Bilirubin-binding FP markers

A small fluorescent protein, UnaG, lights up the muscle fibers of the Japanese freshwater eel, *Anguilla japonica* [109]. UnaG was structurally and spectroscopically characterized by Miyawaki and coworkers in 2013 [110]; it belongs to the fatty acid binding

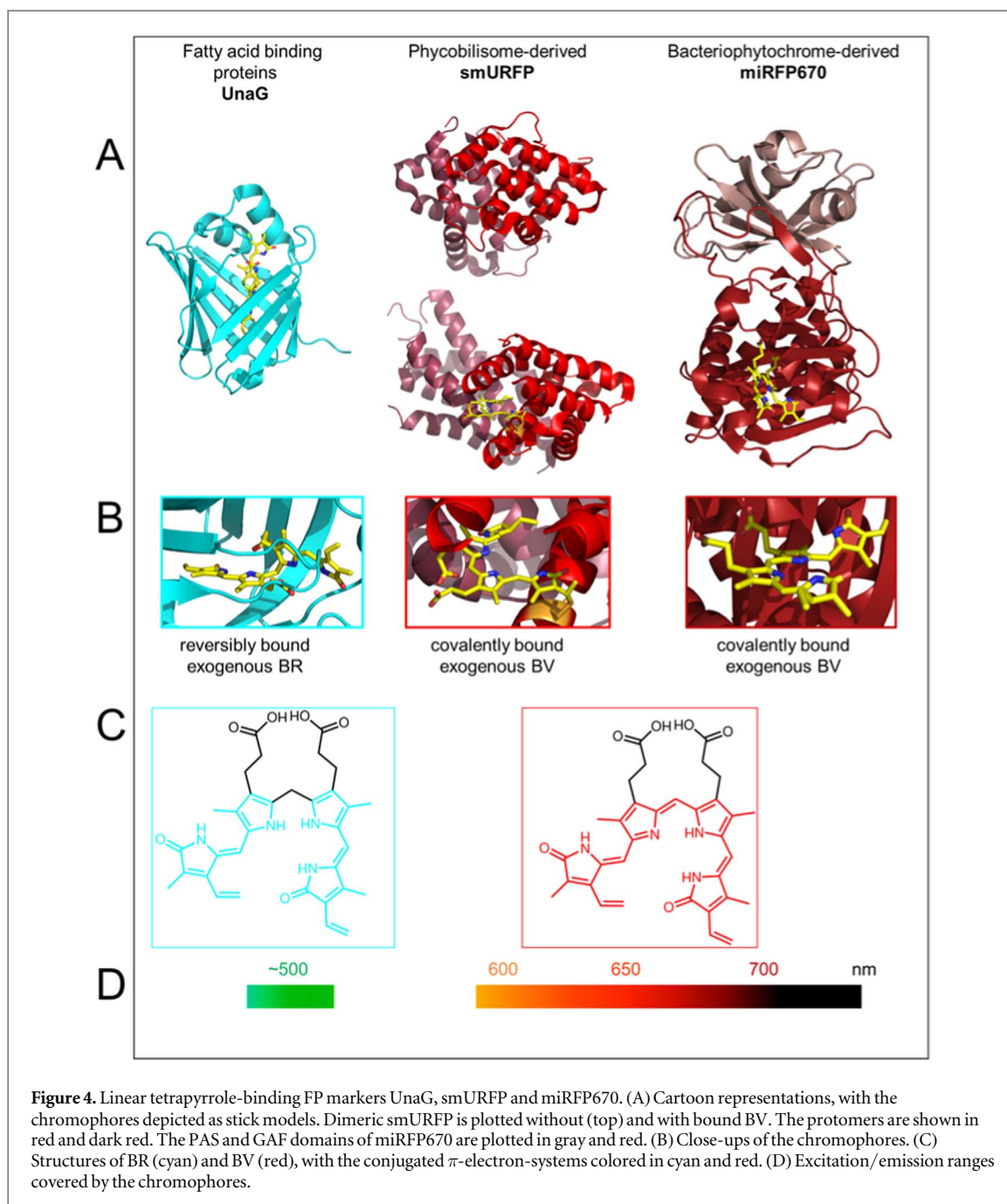
protein (FABP) family and has a molecular mass of 16.5 kDa. Its 139 amino acids fold into a ten-stranded β -barrel that is capped by two α -helices (figure 4). Meanwhile, representatives of this protein class have been identified in other eel species as well [111–113]. UnaG binds BR non-covalently with high specificity and affinity ($K_D = 98$ pM) in an interior pocket. BR binding, the rate of which scales with the concentration of BR in the environment, leads to a fluorescence turn-on of the cofactor. Off-switching is due to ligand dissociation, which can be significantly accelerated by photooxidation of UnaG-bound BR, enabling light-controlled clearance of the internal cavity [114]. UnaG has maximal absorbance at 498 nm ($\epsilon = 77,300$ M $^{-1}$ cm $^{-1}$), and strong fluorescence with QY 0.51 with a maximum at 527 nm (table 5), resulting in a molecular brightness comparable to that of EGFP. An enhanced variant, eUnaG, carrying the single-point mutation, Val2Leu, was reported to have a more than two-fold increased brightness in bulk assays with live insect cells [115].

UnaG was first employed in a sensitive fluorometric assay for measuring blood BR levels in clinical analytics [110]. The suitability of UnaG as a fluorescence marker has been demonstrated in a variety of imaging applications [110], including subcellular mapping of bilirubin in live mammalian cells [116]. Furthermore, reporters of protein-protein interactions have been developed based on complementation assays with split UnaG constructs [117].

3.2. Phycobilisome-based FP markers

In 2016, Tsien and collaborators [118] engineered the small ultra-red FP (smURFP) from an allophycocyanin α -subunit. This protein is part of the light harvesting antenna complex (phycobilisome) of the cyanobacterium *Trichodesmium erythraeum* (TeAPC α). The native protein requires a lyase to incorporate PCB, whereas smURFP binds a BV chromophore spontaneously and covalently via a cysteine residue, Cys52, marked in orange in figure 4. Its excitation and emission bands are in the far-red spectral region at 642 and 670 nm, respectively. Forming a tightly bound homodimer with an overall molecular mass of 32 kDa, smURFP is only slightly bigger than GFP and very bright, due to a large (dimer) extinction coefficient (180,000 M $^{-1}$ cm $^{-1}$) and a QY of 0.18, which is quite high for FP markers with a flexible BV tetrapyrrole chromophore (table 5). Moreover, smURFP was attested a high photostability, in fact, the highest one of all FP markers ever investigated in the Tsien lab [118]. Recently, another allophycocyanin-derived protein, BDFP1.5, was reported that is monomeric and has further red-shifted excitation and emission peaks but, unfortunately, much lower brightness [119].

In cell culture studies, supplementation with membrane-permeant BV dimethylester (BVMe $_2$) was



shown to greatly improve chromophore availability and thus the effective brightness of smURFP. Interestingly, the spontaneously formed smURFP dimer incorporates only a single BVMe₂, whereas the tandem dimer consisting of two concatenated protomers binds two of them [118]. Despite its excellent performance *in vitro*, smURFP was not judged effective for whole-animal imaging due to insufficient supply of BV [108, 118].

Recently, Machado *et al* [120] proposed to use smURFP as a self-labeling protein tag, similar to SNAP, CLIP or Halo [8]. As the two carboxylates of the BV chromophore are not recognized by smURFP for binding, they are available for coupling of polyethylene glycol (PEG) linkers tethering cargo molecules. Interestingly, only the mono-substituted

BV-PEG-fluorescein but not BV-(PEG-fluorescein)₂ was covalently attached to the protein.

3.3. Bacteriophytochrome-derived FP markers

Phytochrome photoreceptors are expressed in plants, fungi, cyanobacteria and bacteria to sense the light conditions in their environment [121]. They covalently bind linear tetrapyrroles including P Φ B, PCB or BV to form a photochromic holoprotein. The light-sensing function relies on reversible, photo-induced interconversion between a fluorescent red- and a non-fluorescent far-red-absorbing form, denoted 'Pr' and 'Pfr', respectively. This process involves cofactor photoisomerization, which needs to be suppressed by suitable amino acid mutations to obtain a bright phytochrome-based FP marker with low flickering.

Table 5. Optical properties of linear tetrapyrrole-binding FPs.

	Parental Protein	λ_{Exc} (nm)	λ_{Em} (nm)	ε ($\text{M}^{-1} \text{cm}^{-1}$)	QY	Brightness	References
Fatty acid binding proteins							
UnaG	N/A	498	527	77,300	0.51	39.4	[110]
Phycobilisome-derived proteins							
smURFP	TeAPC α allophycocyanin	642	670	180,000	0.18	32.4	[118]
BDFP1.5	ApcF2 allophycocyanin	688	711	74,000	0.05	3.7	[119]
Bacteriophytochrome-derived proteins							
emiRFP670	RpBphP1	642	670	87,400	0.14	12.2	[131]
miRFP680	RpBphP2	661	680	94,000	0.15	13.6	[131]
emiRFP703	RpBphP1	674	703	90,900	0.09	7.8	[131]
miRFP713	RpBphP2	690	713	99,000	0.07	6.9	[131]
miRFP720	RpBphP2	702	720	98,000	0.06	6.0	[269]
SNIFP	DrBphP	697	720	149,000	0.02	3.3	[155]
mIFP	BrBphP	683	705	65,900	0.07	4.6	[270]
Cyanobacteriochrome-derived proteins							
miRFP670 nano	NpR3784	645	670	95,000	0.11	10.3	[134]

Among the different species, bacterial phytochrome photoreceptors (BphPs) have the lowest-energy electronic transitions, as they incorporate BV as the ligand. Therefore, they are attractive as templates for engineering far-red and NIR FPs. Full-length BphPs are homodimers, with each of the ~ 730 amino acids long protomer chains arranged in several domains [122]. Only the first two domains of the N-terminal photosensory module, denoted Per-Arnt-Sim (PAS) and cGMP phosphodiesterase/adenylate cyclase/Fh1A transcriptional activator (GAF) are required for engineering an FP marker that has ~ 35 kDa molecular mass. The BV cofactor is buried in a pocket in the GAF domain (figure 4) [123], yet covalently (and autocatalytically) attached to a cysteine residue of the PAS domain, which also confers thermodynamic stabilization to the entire structure.

The first bacteriophytochrome-based FPs consisting of 321 amino acids, denoted infrared-fluorescent proteins (IFPs), were engineered in 2009 from a *Deinococcus radiodurans* phytochrome [124]. Subsequently, other markers were engineered from different BphPs [125–129]. Many of these were dimeric and/or showed low brightness in mammalian cells, hampering their use as markers for imaging. Their fluorescence can be enhanced with an external supply of BV [124] or co-expression of heme oxygenase [126] to enzymatically generate BV from heme, which may, however, adversely affect cell metabolism and proliferation [130]. Recently, a variety of monomeric far-red/NIR FPs with excitation and emission in the ranges 642–702 nm and 670–720 nm, respectively, were reported (table 5) [131], some of which had beneficial properties for stimulated emission depletion (STED) microscopy (see section 4.2). A common feature of all BV-based FPs is their low QY (table 5); yet, the relatively high extinction coefficients make them nevertheless quite suitable for cell, tissue and whole-animal imaging. Photoactivatable phytochrome-based FP markers have also been developed [132].

These PS-FPs feature photoinduced transitions from the non-fluorescent Pfr to the fluorescent Pr state; the back-reaction occurs in the dark.

3.4. Cyanobacteriochrome-derived FP markers

Cyanobacteriochromes (CBCRs) are photoreceptor proteins found in cyanobacteria. They are distantly related to bacterial phytochrome-based photoreceptors and offer great opportunities for the development of FP markers in the visible and far-red/NIR parts of the spectrum [133]. Only a single GAF domain binds the linear tetrapyrrole chromophore and permits reversible photoisomerization as in canonical phytochrome photoreceptors, which allows very small, single-domain FP markers to be developed. In 2019, a CBCR-derived, BV-binding far-red FP, miRFP670-nano, was reported [134]. With a polypeptide chain of 147 amino acids, it has a molecular mass of only 17 kDa. However, it is not as bright as its phytochrome-based counterparts [131]. Photoswitchable marker proteins can also be developed from CBCRs by retaining their photoreceptor functionality, as was demonstrated for the red-green switchable biliprotein (RGS protein) from *Synechocystis* sp. PCC6803 [135]. Although RGS is far from being a useful FP marker, it shows the potential of CBCRs as templates for further engineering of far-red/NIR FP markers.

4. Advanced imaging with FP markers

Basic concepts of fluorescence microscopy and the operating principles of advanced imaging methods have been reviewed extensively [3, 5, 19, 136–140]. The choice of the most effective imaging approach for a particular experiment depends on the nature of the sample (live or fixed, dimensions of the specimen), the resolution (in time and space) required for answering a biological question, the type of data to be recorded (plain imaging in one or more channels or dynamic imaging, e.g., to monitor interactions between

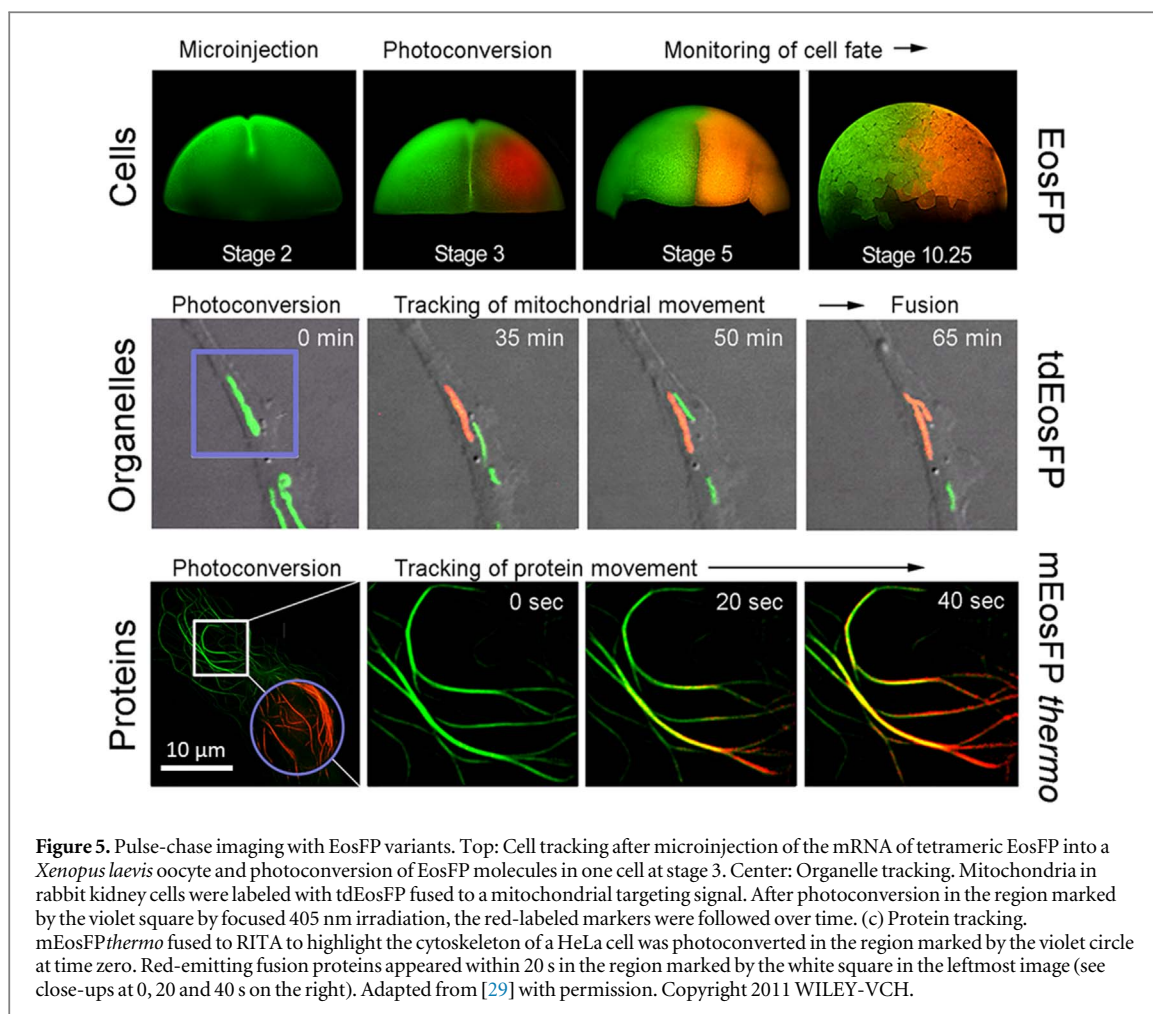


Figure 5. Pulse-chase imaging with EosFP variants. Top: Cell tracking after microinjection of the mRNA of tetrameric EosFP into a *Xenopus laevis* oocyte and photoconversion of EosFP molecules in one cell at stage 3. Center: Organelle tracking. Mitochondria in rabbit kidney cells were labeled with tdEosFP fused to a mitochondrial targeting signal. After photoconversion in the region marked by the violet square by focused 405 nm irradiation, the red-labeled markers were followed over time. (c) Protein tracking. mEosFP^{thermo} fused to RITA to highlight the cytoskeleton of a HeLa cell was photoconverted in the region marked by the violet circle at time zero. Red-emitting fusion proteins appeared within 20 s in the region marked by the white square in the leftmost image (see close-ups at 0, 20 and 40 s on the right). Adapted from [29] with permission. Copyright 2011 WILEY-VCH.

different biomolecules), the type of analysis (qualitative, quantitative), and the equipment and experience available in the lab [141]. It is crucially important to select a fluorescence marker that best supports the selected imaging method. In the following, we will briefly introduce a few common fluorescence-based imaging techniques, discuss the essential properties of FP markers that are suitable for these methods and present selected applications.

4.1. Confocal laser scanning microscopy (CLSM)

A regular confocal microscope uses a diffraction-limited, focused Gaussian laser beam (Airy spot) as a probe to raster-scan the sample in the focal plane, exciting fluorophores pixel by pixel. Thus, the image resolution depends on the size of the probe (spot). As a time-sequential, single-point technique, CLSM is relatively slow when taking images with many pixels [142]. To achieve sampling at higher speeds, spinning disk confocal microscopy utilizes many (ca. 1,000) foci in parallel [143]. A confocal pinhole in the detection pathway is essential for CLSM; it rejects light from out-of-focus planes and thus enables optical sectioning.

Fluorescence markers should be chosen according to the available laser wavelengths to ensure effective excitation and optimal SBR. Furthermore, important

parameters for selection are brightness and photobleaching resistance [138]. For color (lifetime) multiplexing, it is preferable that excitation and/or emission spectra (lifetime decays) of the individual dyes are markedly different to minimize channel cross-talk. As molecular oxygen is one of the key players responsible for photobleaching, adding oxygen scavengers and/or triplet quenchers to the specimen reduces build-up of reactive oxygen species and can often greatly improve survival of both fluorophores and live cells or organism during light exposure [144].

Green-to-red PC-FPs enable pulse-chase imaging, a powerful technique to observe dynamics in live cells, tissues, and organisms that is related to fluorescence recovery after photobleaching (FRAP) and similar approaches [145]. A live specimen expressing a protein of interest fused to a PC-FP is imaged in the green channel. Next, a subregion is targeted with a pulse of 405-nm laser light, and the red-converted, tagged molecules are followed (chased) in the red color channel without interference from newly expressed green-emitting proteins. Examples are shown in figure 5.

More recently, optical clearing methods such as ‘Clear Lipid-exchanged Acrylamide-hybridized Rigid Imaging/Immunostaining/*In situ* hybridization-compatible Tissue-hydrogel’ (CLARITY) [146] have been developed that render whole rodent brains

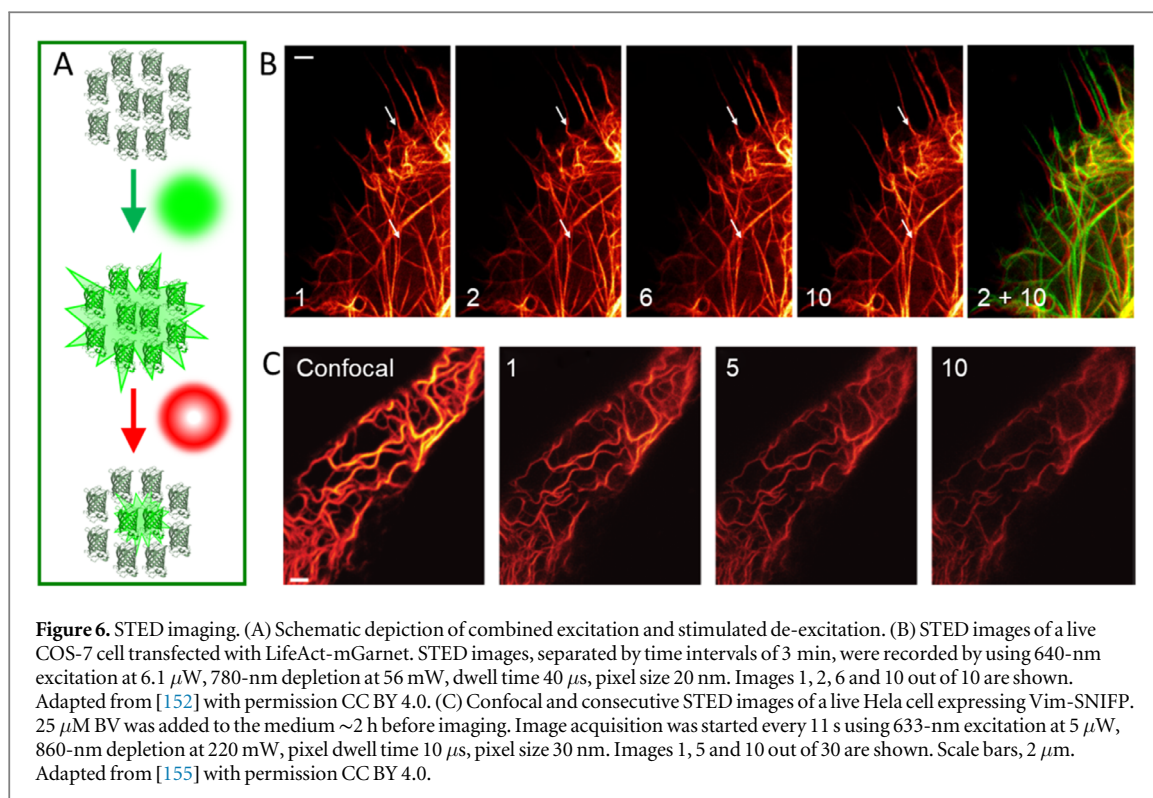


Figure 6. STED imaging. (A) Schematic depiction of combined excitation and stimulated de-excitation. (B) STED images of a live COS-7 cell transfected with LifeAct-mGarnet. STED images, separated by time intervals of 3 min, were recorded by using 640-nm excitation at $6.1 \mu\text{W}$, 780-nm depletion at 56 mW, dwell time $40 \mu\text{s}$, pixel size 20 nm. Images 1, 2, 6 and 10 out of 10 are shown. Adapted from [152] with permission CC BY 4.0. (C) Confocal and consecutive STED images of a live HeLa cell expressing Vim-SNFP. $25 \mu\text{M}$ BV was added to the medium ~ 2 h before imaging. Image acquisition was started every 11 s using 633-nm excitation at $5 \mu\text{W}$, 860-nm depletion at 220 mW, pixel dwell time $10 \mu\text{s}$, pixel size 30 nm. Images 1, 5 and 10 out of 30 are shown. Scale bars, $2 \mu\text{m}$. Adapted from [155] with permission CC BY 4.0.

transparent to prepare them for fluorescence imaging. Unlike EGFP, the variant muGFP is able to withstand these harsh chemical treatments and remain fluorescent [147].

4.2. Stimulated emission depletion (STED) microscopy

In essence, STED microscopy is CLSM with a ‘sharpened’ probe beam, so that the pixel step size can be reduced to visualize fine details. This is achieved by scanning with two spatially and temporally overlaid beams, (1) a tightly focused Airy spot to excite fluorophores, and (2) a red-shifted beam with toroidal (doughnut-shaped) intensity profile in the focal plane and zero intensity in its center. This high-power depletion (or STED) beam de-excites fluorophores outside the central region of the Airy spot by stimulated emission, thereby effectively ‘sharpening’ the probe used for raster scanning of the sample (figure 6(A)).

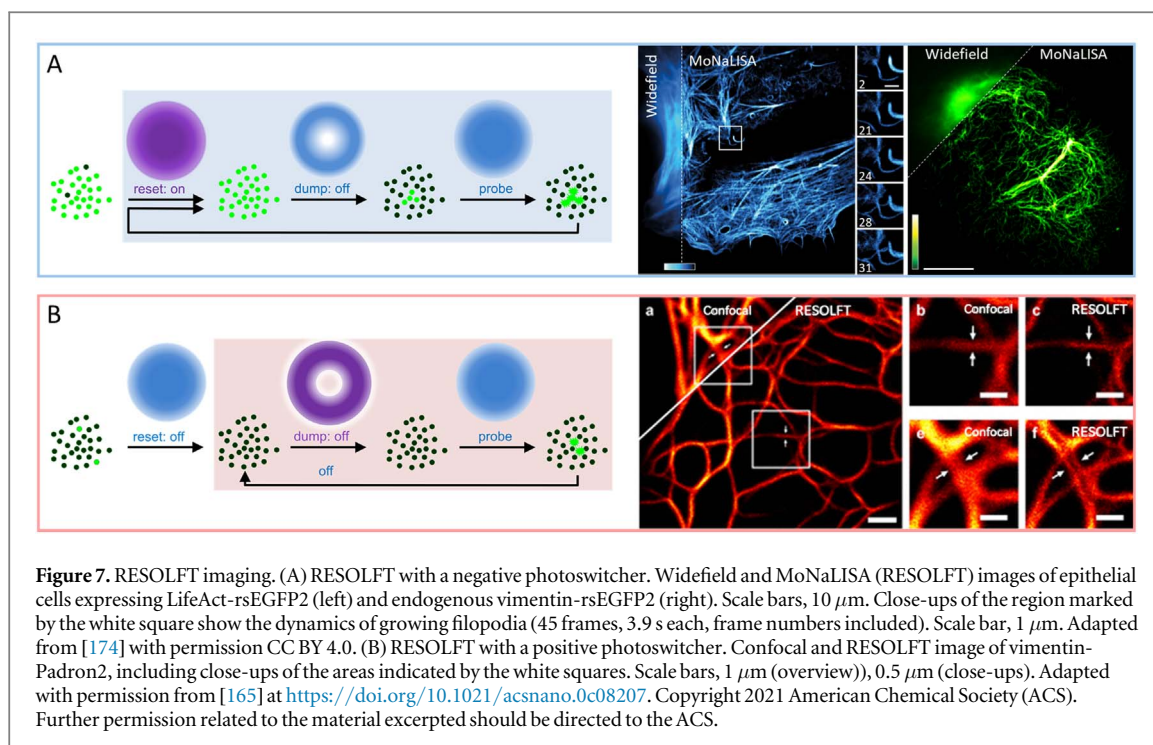
As stimulated emission is a fundamental phenomenon, any fluorophore is in principle suited for STED microscopy. However, fluorescence labels should be extremely photostable to withstand the high laser power of the STED beam (ca. $5 \text{ MW}/\text{cm}^{-2}$ [148]) needed for efficient depletion. At the same time, depletion should occur at the red edge of the fluorophore’s emission spectrum to minimize re-excitation by the STED beam. Moreover, the smaller pixel spacing implies that fluorophores have to endure many excitation-depletion cycles during scanning. Some organic dyes are very resistant to photodestruction and thus excellent for STED imaging. Nevertheless, STED has

also been employed successfully in live-cell imaging with a range of far-red emitting GFP-type FPs [149–154] as well as tetrapyrrole-binding FPs [155] (figures 6(B), (C)). Monomeric NIR FPs derived from *Rhodospseudomonas palustris* including emiRFP670, miRFP670-2 and miRFP680, enabled STED imaging in live U2OS cells with a resolution approaching 40 nm, even without adding exogenous BV [131].

4.3. Reversible saturable optical fluorescence transitions (RESOLFT) microscopy

Selective depletion of fluorescence markers in the wings of the excitation spot, which is key to the resolution enhancement of STED microscopy, can be achieved in other ways than via stimulated emission from the excited singlet state, e.g., by exploiting triplet state transitions [156, 157]. All these ‘STED-like’ approaches are subsumed under RESOLFT microscopy, as reversible light-inducible transitions between saturable energy levels play essential roles for all of them [158–160]. In this context, fluorophores that can be driven by light between (long-lived) bright and dark states are most attractive [158, 159, 161]. Their key advantage is that depletion of the emissive state requires only moderate intensity thanks to the small spontaneous transition probabilities, whereas regular STED imaging uses high laser power to ensure that depleting transitions outcompete fluorescence transitions occurring on nanosecond time scales.

PS-FPs are convenient probes for RESOLFT imaging, as they inherently feature long-lived on- and off-states with state lifetimes ranging from tens of seconds to hours [49, 162], and can be switched selectively back



and forth between these states multiple times by light irradiation [91]. The scanning procedure uses a ‘reset-dump-probe’ sequence, carried out at each and every pixel, the details of which depend on the switching mode (positive or negative, see section 2.2.2).

For RESOLFT imaging with negative photoswitchers, PS-FPs are first switched on by a ~ 400 nm (for a green-emitting PS-FP) Airy-shaped pulse of activating light (reset, $T^H \rightarrow C^-$, figure 7(A)) [91, 163]. Next, the donut-shaped depletion beam (~ 480 nm) switches off all fluorophores in the periphery of the targeted spot (dump, $C^- \rightarrow T^H$). Only fluorophores in the center of the depletion beam remain in the fluorescent C^- state, and can subsequently be probed by a short pulse of ~ 480 nm Airy-shaped excitation light (probe). Note that the depletion and probe beams have the same wavelength, but their beam profiles and intensities differ (figure 7(A)). The sequence repetition rate (scan speed) is limited by the transition rate between the on- and off-states. Typically, off-switching with blue light is 2–3 orders of magnitude slower than on-switching (for comparable light intensity), rendering off-switching the rate-limiting step [164].

Positive photoswitchers are typically non-fluorescent in thermal equilibrium, as chromophores reside mainly in the T^- configuration. For RESOLFT imaging, they are first reset, *i.e.*, photoactivated by an Airy spot of ~ 480 nm light (for a green-emitting PS-FP) and isomerize/protonate to yield non-fluorescent C^H chromophores, which are in thermal equilibrium with the fluorescent C^- species (figure 7(B)). Next, the donut-shaped depletion beam is applied to induce $C^H \rightarrow T^-$ transitions in the periphery of the Airy spot (dump, ~ 400 nm). Non-fluorescent C^H chromophores only remain in the central region, and are

subsequently excited by the probe beam at ~ 480 nm to collect the image. Importantly, this illumination scheme requires only two beams, an Airy-shaped ~ 480 nm beam and a doughnut-shaped ~ 400 nm depletion beam (figure 7(B)). In practice, the sample can be scanned simultaneously with both beams, which speeds up image acquisition, as was shown by Konen *et al* [165] with the positive photoswitcher Padron2 (figure 7(B)).

A high molecular brightness of the fluorophores is always beneficial for a good SBR; however, it is not as critical for RESOLFT as for imaging methods based on single-molecule detection (see section 4.5), as several molecules are typically detected in each pixel. Initially, mainly the green-emitting rsEGFP and rsEGFP2 were employed for RESOLFT imaging, requiring ~ 400 -nm light for photoswitching [164, 166, 167]. Wang *et al* [168, 169] introduced the Met168Ala mutation into the PC-FP mMaple3 to endow it with photoswitching capability. In addition, they replaced the histidine of the chromophore triad by essentially all other amino acids to generate the GMars series of green-emitting PS-FPs. Among those variants, GMars-Q and GMars-L were found to retain ~ 10 and $\sim 15\%$ of their fluorescence for more than 2,000 switching cycles, which was shown to be beneficial for RESOLFT nanoscopy in live cells. It is noteworthy, however, that the low apparent switching fatigue of GMars-Q does not reflect photo-physical robustness but derives from efficient shelving of FPs in dark states [170].

Orange and red PS-FPs often suffer from small switching contrast or poor chromophore maturation [171, 172]. Penachetti *et al* [173] engineered optimized red-emitting PS-FPs starting from the FP Fusion Red and demonstrated their suitability for live-cell

RESOLFT microscopy using molecular nanoscale live imaging with sectioning ability (MoNaLISA) microscopy. In this massively parallelized RESOLFT approach, a 2D-periodic multi-focal (3,600 foci) light pattern (488 or 510 nm), generated by a multi-lens array, induces patterned on-switching of the red-emitting PS-FPs. Subsequently, a 2D-periodic (590-nm) light pattern made with crossed line gratings switches FPs located in the periphery of the foci into the off-state, so that fluorophores remain in the on-state in the center and can be read out with a third, multi-focal light pattern at 590 nm. The same approach has also been successful with green-emitting rsEGFP2 using wavelengths of 405 and 488 nm (figure 7(A)) [174].

4.4. Widefield and structured illumination microscopy (SIM)

Widefield microscopy is conceptually the simplest microscopy technique, involving light sources that illuminate the entire field of view and detection by a camera (or just by eye). It places no special demands on the fluorophores, so bright and photostable FPs such as EGFP or mCherry are well suited as markers. Based on widefield microscopy, SIM is a sophisticated modality that offers roughly twice-enhanced resolution over regular imaging [175]. By illuminating the specimen with a fine periodic line pattern that can still be optically resolved, a beat pattern (Moiré fringes) emerges in the resulting image. It carries information about spatial frequencies of the object above the diffraction limit (cut-off frequency of the optical transfer function), which can be recovered from the acquired image since the structure of the illumination pattern is known. As the spatial frequencies of both object and illumination patterns are limited by diffraction, the resolution enhancement of SIM is roughly twofold (assuming a small Stokes shift). For image reconstruction, 2D (3D) SIM requires at least nine (15) separate camera exposures of the region of interest, during which the sample must remain quasi static. Therefore, SIM has initially been geared toward fixed-cell imaging. However, live-cell imaging is quite feasible thanks to the high frame rates of modern cameras [176–178].

By exploiting the non-linearity of the object's emission response to the excitation light, even greater resolution enhancements can be achieved, as originally shown with saturated structured illumination microscopy (SSIM) [148, 179, 180]. This approach requires extremely photostable fluorophores and is not compatible with FP markers. A non-linearity can also be created with PS-FPs, however, which can be reversibly driven into saturation in their dark and bright states by irradiation at a suitably chosen wavelength [176, 181–183], as in RESOLFT microscopy. Using the PS-FP Dronpa, Rego *et al* [181] achieved 50-nm image resolution with non-linear SIM (NL-SIM). More recently, Betzig and collaborators [184]

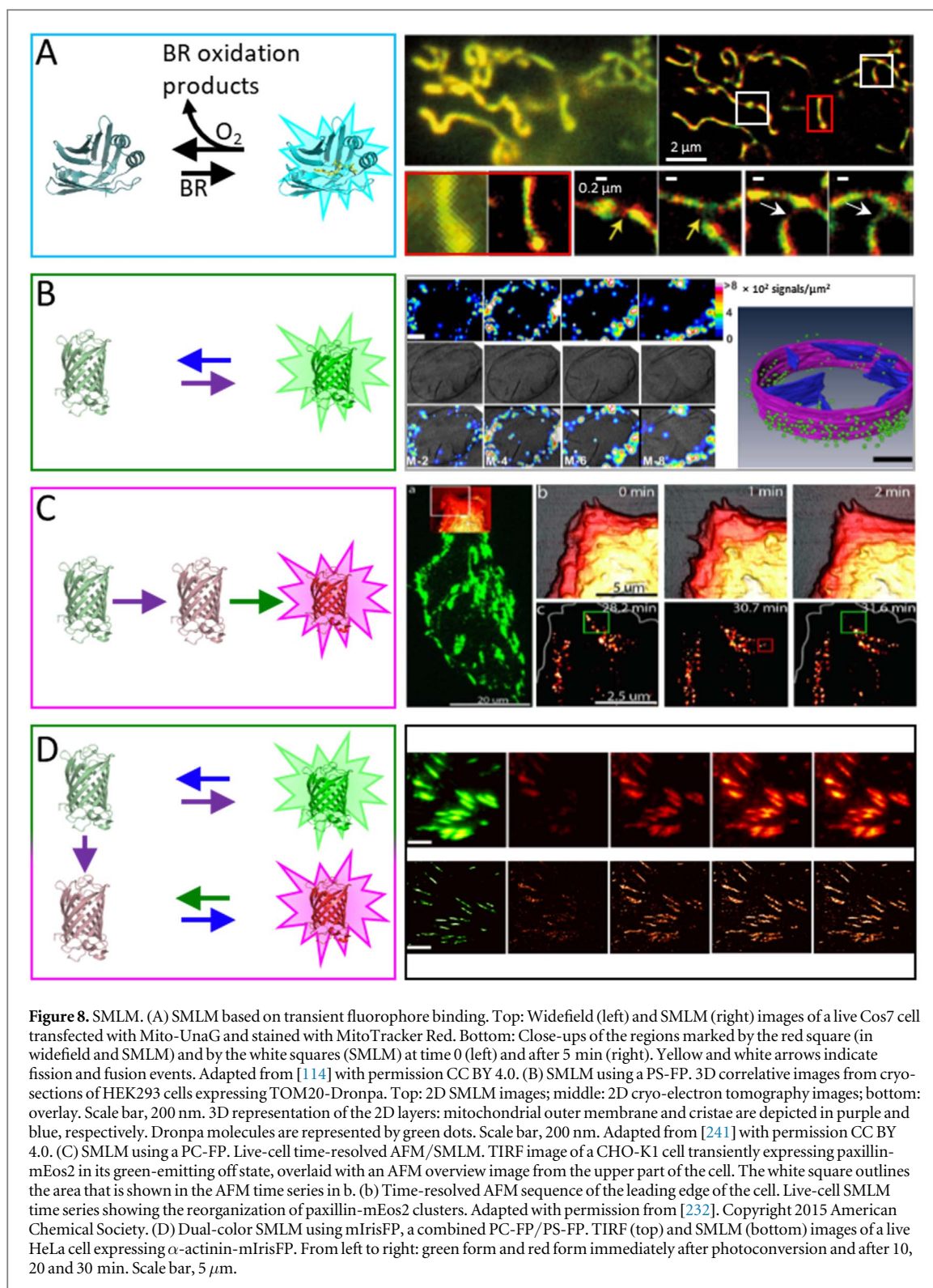
introduced patterned activation NL-SIM with the PS-FP marker Skyran-NS for capturing live-cell movies at 60-nm image resolution.

4.5. Single-molecule localization microscopy (SMLM)

SMLM is the generic term comprising various advanced techniques based on localization of individual fluorescence emitters, including photoactivated localization microscopy (PALM) [185, 186], stochastic optical reconstruction microscopy (STORM) [187] and direct STORM [188], and point accumulation for imaging in nanoscale topography (PAINT) [189–191]. SMLM requires the use of fluorophores that do not emit photons continually but intermittently and randomly from a given location of the object [140]. This can be achieved either by transient binding of continuously emitting fluorophores as in PAINT (figure 8(A)) or by using photoactivatable fluorophores, i.e., fluorophores that can be turned on by light irradiation (figures 8(B)–(D)) [185–188]. A SMLM image is reconstructed from a sequence of ca. 10^2 – 10^4 widefield images. Each individual image contains only a small number of active emitters, so that overlap of their individual spots is not an issue, and their location can be precisely determined as the center of gravity of their image spot.

Photoactivatable FPs are convenient markers for SMLM. From a large pool of FP markers in the sample, only a few are photoactivated in each image by irradiating with weak activating light. They are excited, localized and photobleached, while the majority of them resides in the off-state. For precise localization in SMLM, the FPs should have high molecular brightness and resistance to photobleaching, so that a large number of photons can be detected [192]. Moreover, the contrast between the emission of on- and off-states should be large to ensure minimal background generated by the huge pool of inactive FPs. PC-FPs typically yield much better contrast than PS-FPs as they appear in a different color channel after photoconversion [91]. In practice, detection of ca. 100 photons per single fluorophore is sufficient for ca. tenfold resolution enhancement, as the localization precision scales with the inverse root of the number of photons. Notably, this also requires a sufficient labeling density.

For SMLM with GFP-type PS-FPs, the absorption bands of the bright and dark species should be well separated, so that on-off and off-on transitions can be driven selectively (figure 8(B)). Negative photo-switchers (with C^- as the fluorescent form) yield the highest contrast for $pK_{cis} \ll pH_{sample} \ll pK_{trans}$ (see section 2.2.2). When exciting the fluorophores, the laser also switches their emission off again, albeit with low probability. If the QY for off-switching is large, the photon budget is chopped up into multiple short, time-separated photon 'bursts' from the same FP in



different image frames, reducing the localization precision and complicating molecule counting [193, 194].

Typically, PS-FPs require two different illumination wavelengths for fast on- and off-switching. The green-emitting SPOON [90], however, switches off by 488-nm excitation and switches on again swiftly by thermal activation, enabling SMLM with only a single 488-nm laser.

GFP-type PC-FPs are excellent tags for SMLM because they ideally undergo only a single activation

step before registration (and subsequent photobleaching). Green-to-red PC-FPs (table 4) such as members of the EosFP clade [195] are presently the optimal choice for SMLM (figures 8(C), (D)). As they are expressed in the green state, i.e., the off-state with respect to detection at wavelengths in the red spectral region, their proper expression by the cell can be examined by taking an image with green emission. Photoconversion occurs with weak 400-nm light but is

negligible for excitation of the green or red species. However, problems may arise if the PC-FP displays long-lived dark states in the red-emitting form. For example, photoactivated mEos2 was found to undergo repeated transitions to long-lived dark states, which can give rise to errors due to multiple counting of the same molecule [196, 197].

In 2006, Betzig *et al* [186] used fusion constructs with d2EosFP [54] to image vinculin at focal adhesions, actin within a lamellipodium, and the distribution of the retroviral protein Gag at the plasma membrane. Zhou *et al* [198] elucidated how motor proteins ensure the supply of vesicles to the hyphal tip of filamentous fungi by quantitative SMLM of live *Aspergillus nidulans* fungi expressing mEosFP*thermo* fused to the chitin synthase ChsB. Combined PC-FPs/PS-FPs such as mIrisFP enable pulse-chase experiments in two color channels (figure 8(D)) [104]. For completeness, we mention that PA-GFP and related variants (table 3) can also be used for SMLM but are inconvenient because they are only visible after photoactivation.

UnaG from the Japanese freshwater eel *Anguilla japonica* displays intermittent emission without light-induced switching to the on-state; only the off-state is under light control [114]. UnaG's usefulness for SMLM was demonstrated with fusion proteins labeling the ER (UnaG-Sec61 β), vimentin filaments (Vim-UnaG), and clathrin-coated pits (UnaG-CLC, clathrin light chain) in fixed Cos7 cells (figure 8(A)) [114]. With a high excitation intensity of $\sim 300 \text{ W cm}^{-2}$ at an exogenous BR concentration of $\sim 1 \mu\text{M}$, most FPs were kept in the off-state; only a small fraction of BR-bound and thus fluorescent UnaG markers remained. Each of them emitted $\sim 1,200$ photons on average before off-switching, which is comparable with EosFP [199] and the dye Atto 488 [200] and thus yields a comparable localization precision. For surface-immobilized UnaG molecules, a localization precision of $\sim 12 \text{ nm}$ and a resolution of $\sim 28 \text{ nm}$ (full-width at half-maximum) in the lateral directions was reported. In a follow-up study, an improved variant, eUnaG, with an even higher photon budget was presented [115].

4.6. Light sheet microscopy

Light sheet microscopy was introduced already more than 100 years ago [201, 202] and re-discovered in 2004 as a superb method to visualize 'large' specimens (ca. 1 mm^3) such as model organisms with cellular resolution [203]. Its key distinguishing feature is the uncoupling of the optical axes of excitation and detection. Only a single slice within the sample is illuminated, and the fluorescence excited within that slice is collected in a perpendicular direction (figure 9(A)). Therefore, photobleaching and phototoxicity (in live samples) are greatly reduced. For optimal sectioning, various ways have been devised to form a light sheet with minimal thickness over a

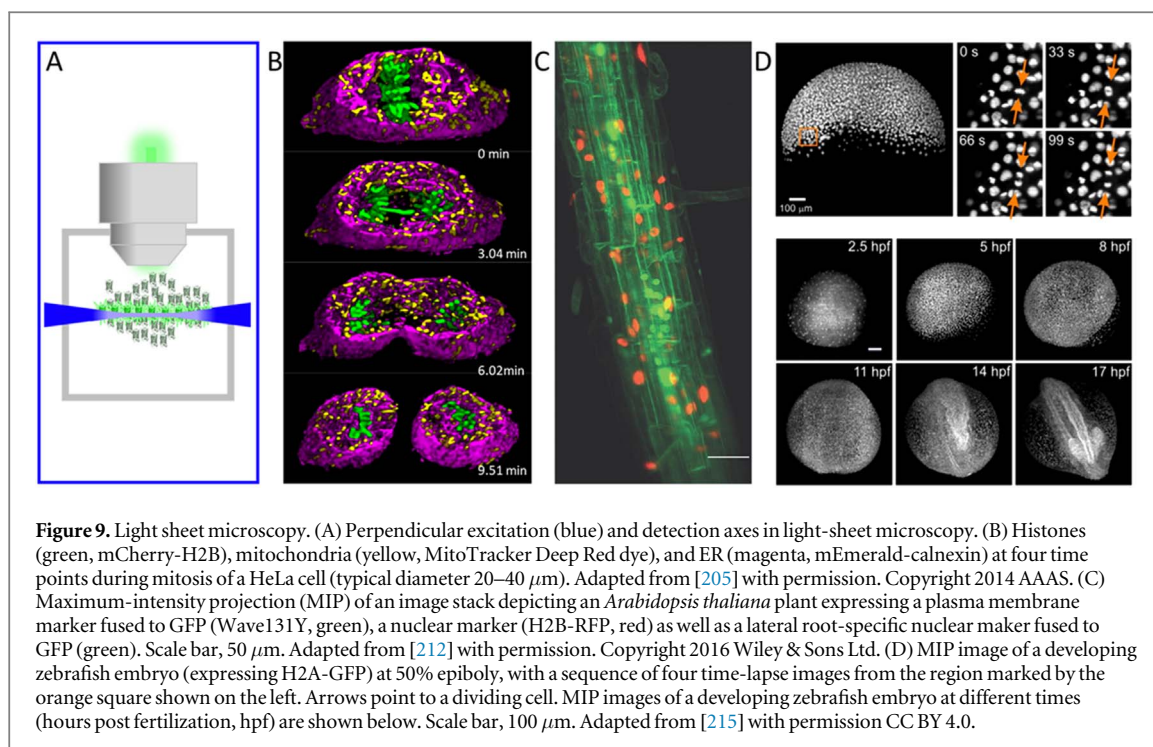
specified longitudinal distance. The simplest approach uses a cylindrical lens; better performance can be achieved, though, with structured illumination using digital scanning of Gaussian, Bessel, Airy, and lattice beams [203–207]. Multi-view imaging of a specimen from different angles combined with subsequent image fusion takes more effort but yields isotropic resolution [208]. Light sheet microscopy offers *in-vivo* 3D+t visualization of developing embryos over hours and days with high speed and minimal biological perturbation [209–211]. More recently, subcellular imaging has been demonstrated using lattice light sheet excitation (figure 9(B)) [205].

Light sheet microscopy has no special demands on the FP markers, it even works quite well with first-generation red FPs such as mCherry. For imaging live organisms, FPs with excitation and emission in the red to far-red region are preferable due to lower scattering and autofluorescence at longer wavelengths. Moreover, continual replenishment of genetically encoded markers by live organisms greatly alleviates photobleaching. GFP- and RFP-fusions have been used to image plasma membranes and cell nuclei in *Arabidopsis* plants (figure 9(C)) [212]. Developmental studies on various model organisms have also been reported, including studies on the transparent zebrafish (*Danio rerio*) embryo, with GFP fusions for labeling cell nuclei (figure 9(D)) [213–215], the heart [216] or cells of the developing eye [217].

4.7. Super-resolution optical fluctuation imaging (SOFI)

Optical microscopy methods are mostly based on capturing the intensity distribution in the image. SOFI, by contrast, yields super-resolved images (and background removal) through higher-order statistical analysis of temporal fluctuations (intermittency) of the photon emission from individual fluorophores [218, 219]. Like SMLM, SOFI is a purely software-based approach that post-processes time sequences of fluorescence images (for an in-depth comparison of SMLM and SOFI, see [220]). SOFI requires fluorophores that switch stochastically between different intensity levels, and the image magnification must be such that the image of a single molecule extends over several pixels.

FPs show intensive blinking on multiple time-scales [66], originating from chromophore dynamics including *cis-trans* isomerization upon excitation (see section 2.2.2) [38, 50, 65]. Those intrinsic fluorescence fluctuations in the red FPs TagRFP, TagRFP-T, and FusionRed have been used for SOFI imaging in live HeLa cells [221]. Typical photoswitchers, i.e., PS-FPs such as Dronpa [222], rsTagRFP [222] or SkyJan-S [223] have been employed in photochromic stochastic optical fluctuation imaging (pcSOFI). Upon excitation with 488-nm (561 nm for rsTagRFP) laser light, the C⁻ species of the chromophore fluoresces or switches to



the dark state, T^H , with a low probability. With the same wavelength, T^H is also excited and isomerizes back to the fluorescent C^- state. We note that the absorption of T^- at the excitation wavelength is markedly lower than that of C^- . But because on-switching is orders of magnitude more efficient than off-switching [224], there is continual activation and deactivation of PS-FPs (blinking).

Typically, the extent of the intensity fluctuations limits the resolution enhancement of SOFI in biological samples [225]. Mo *et al* [226] discovered that emission fluctuations of TagRFP-T were significantly enhanced by the presence of Dronpa in close proximity, a phenomenon they termed fluorescence fluctuation increase by contact (FLINC). They also provided evidence that FLINC was mediated by amino acid residues on the Dronpa surface and not by the chromophore. In a follow-up study, they fused a non-fluorescent Dronpa mutant with TagRFP-T through an 8-amino-acid linker. The resulting μDpTT showed robust single-molecule fluctuations and was successfully employed for multicolor pcSOFI together with Dronpa [227].

4.8. Fluorescence microscopy in correlative imaging

In correlative microscopy, multiple imaging modalities are employed in combination to probe the same sample, either simultaneously or sequentially [228, 229]. Their different contrast mechanisms, resolution and other properties provide complementary information, and correlative approaches yield more information than is obtained from separate experiments. A simple example of correlative imaging is (simultaneous) confocal and super-resolution fluorescence microscopy in two color channels [230, 231].

For live-cell imaging on the nanoscale, Odermatt *et al* [232] used atomic force microscopy (AFM) and SMLM in a correlative approach (figure 8(C)). By recording a series of AFM images of the leading edge of a live CHO-K1 cell, they studied filopodia protrusion with subsequent lamellipodia extension. As the cell was also transiently transfected with a paxillin-mEos2 construct, SMLM imaging allowed simultaneous recording of the concomitant reorganization of focal adhesions via paxillin-mEos2. Gómez-Varela *et al* [233] combined AFM with SIM to image the plasma membrane transporter, MCT1, tagged with EGFP, in the plasma membrane of CRISPR/Cas9 genome-edited human U2OS cells. Navikas *et al* [234] performed live-cell scanning ion-conductance microscopy (SICM) combined with SOFI to image the cytoskeletal actinin dynamics of COS-7 cells. Correlative STED, PALM and (‘universal’) PAINT allowed imaging of dendritic spines on live hippocampal primary neurons [235]. Cytosolically expressed GFP served as a volume marker of cell morphology, while mEos3.2 (for SMLM) and Atto 647N (for STED) were employed for super-resolution imaging of several prominent synaptic proteins, including the scaffold protein PSD95 and the AMPA receptor subunits GluA1 and GluA2.

Correlative light-electron microscopy (CLEM) is an attractive approach due to the combination of very different contrast mechanisms. It allows specific, fluorescently labeled biomolecules of interest to be resolved on a canvas depicting the high-resolution ultrastructure of the specimen obtained by EM. Sample preparation can be intricate, however, involving chemical fixation with paraformaldehyde and/or glutaraldehyde, staining with osmium tetroxide, dehydration with ethanol and embedding in epoxy resins

Table 6. Optical properties of FPs upon two-photon excitation ($S_0 \rightarrow S_1$ transition, per chromophore) at wavelengths > 700 nm.

FP	λ_{2P-Exc} (nm)	σ_2^a (GM)	σ_2^b (GM)	References
eBFP2.0	750	13	9.2	[248]
Cerulean	858	23	13	[248]
eGFP	927	39	30	[248]
EosFP (green)	1,000	19	13.3	[247]
tdTomato	1,050	108	60	[249]
DsRed	1,050	103	73	[248]
mCherry	1,080	27	6.4	[248]
mKate2	1,140	72	30	[248]

^a Two-photon absorption cross-section.

^b Two-photon brightness, $\sigma_2 \times QY$.

such as Epon [236]. Fortunately, a few FPs can withstand such harsh sample treatment, including mWasabi, CoGFP variant 0 and mCherry2 [236], mKate2 [237], and the photoconvertible mEos4a and mEos4b [238] as well as mEosEM [239]. Watanabe *et al* [240] combined scanning EM with STED microscopy to image the mitochondrial outer membrane protein, TOM20, in ultrathin sections of fixed *Caenorhabditis elegans* specimens embedded in glycol methacrylate.

CLEM at cryogenic temperatures (cryo-CLEM) yields optimal structure preservation through vitrification (fast crystal-free freezing) of the specimen, so chemical fixation and contrast enhancement procedures can be circumvented. Liu *et al* [241] combined cryo-EM with cryo-SMLM and found as an added benefit reduced photobleaching of the PS-FP Dronpa and hence a higher photon budget (figure 8(B)). Moser *et al* [242] demonstrated that structures in thicker parts of the cell can be imaged by cryo-SOFI due to its ability to suppress out-of-focus signals (optical sectioning). Cryo-SOFI was fully compatible with cryo-EM and yielded a similar image resolution as cryo-SMLM [243, 244], but with a several-fold lower laser intensity.

4.9. Fluorescence microscopy with two-photon excitation

In this final application section, we briefly discuss the use of two-photon laser scanning microscopy (2P-LSM) of cells and tissues expressing genetically encoded FP markers. All other imaging techniques mentioned so far are based on absorption of a single photon for fluorescence excitation. By contrast, 2P-LSM involves the simultaneous absorption of two low-energy (long-wavelength) photons for fluorescence excitation, which can be achieved with tightly focused, femto- or picosecond pulses from high-power lasers (typically Ti:sapphire lasers). Key advantages are the intrinsic axial sectioning, which allows 3D raster scanning without a confocal pinhole, and the reduced autofluorescence and scattering when using NIR excitation, enabling deeper tissue penetration. The required excitation power is orders of magnitude

greater than for one-photon microscopy, and optimal imaging conditions have to be chosen to avoid excessive photobleaching [245, 246]. In table 6, we have listed various GFP-type proteins useful for 2P-LSM together with their peak wavelength, corresponding 2P excitation cross section, σ_2 , and the resulting molecular brightness value, σ_2 times QY. More data can be found in [247–249].

5. Conclusions

The introduction of genetically encoded FPs has enabled molecule-specific labeling using comparatively simple molecular biology approaches. Here we have reviewed two classes of genetically encodable FPs, GFP-type proteins and tetrapyrrole-binding proteins, which can function—within their limitations—as self-sufficient, autofluorescent probes. We have discussed their specific properties that make them useful as markers for a range of advanced fluorescence imaging methods. Genetically encodable FPs are remarkably convenient tools and thus have become indispensable for live-cell and organismal imaging. However, expressing artificial genes can be a severe perturbation to a living system, especially when using transient transfection methods, which yield strong overexpression of the FP marker. While this is advantageous for achieving bright images, great caution has to be exercised to avoid artifacts resulting from marker expression.

Overexpression artifacts can be avoided, however, thanks to tremendous advances in our ability to target and edit specific genes within the genome in recent years. Most prominently, the CRISPR/Cas9 approach [250] offers a simple yet powerful tool to introduce a FP domain at a specific locus, making FP marker labeling even more powerful. Gene editing can make sure that expression levels are native-like, which may result in new problems, however. Physiologically, the labeled gene of interest is oftentimes only expressed in small copy numbers, orders of magnitude below transient expression [251]. This can pose severe challenges for imaging and requires microscopes with highest sensitivity and the brightest FP markers available. Thus, novel genetically encodable FPs with higher brightness, suitable absorption/emission and photoactivation properties, and a large photon budget will continue to be in high demand in the future. Especially the development of advanced far-red markers will remain a hot topic in view of the benefits of long-wavelength light for imaging, i.e., low absorption and scattering in the range between 700 and 1300 nm. In this effort, we expect to see further progress especially with BV-binding FPs, as GFP-type proteins have limitations imposed by their smaller *p*-HBI chromophores.

Finally, we briefly allude to other platforms of genetically encoded biomarkers that, however, require

an external supply of synthetic dyes. Therefore, their application is limited to fixed samples and, if membrane-permeant dyes are used, live cells as well, but they have clear benefits in many applications due to the significantly better photophysical properties, especially brightness and photostability, offered by excellent synthetic dyes. Like FPs, chemical tags (e.g., Halo, SNAP/CLIP, smURFP) [12–14, 120] can be expressed as fusion proteins and can bind bright synthetic fluorophores via specific functional groups. Most exciting are also RNA aptamer tags [15–17, 252], tiny RNA structures that bind so-called turn-on fluorophores, which emit strong fluorescence upon aptamer binding. With these novel tools, researchers can finally benefit from genetic encoding of fluorescence markers also on the RNA level. We are convinced that the quest for bright, selective and sophisticated optical fluorescence markers for biological imaging will continue to be a hot research topic for years to come.

Acknowledgments

There are no conflicts of interest to declare. We have made every effort to cite all relevant publications and apologize to those colleagues whose work was not included due to space constraints or oversight. We acknowledge funding by the Helmholtz Association, program Materials Systems Engineering (MSE), the Karlsruhe School of Optics and Photonics (KSOP) and the Deutsche Forschungsgemeinschaft (SFB 1324, project Z02 and GRK 2039).

Data availability statement

No new data were created or analysed in this study.

ORCID iDs

Karin Nienhaus  <https://orcid.org/0000-0002-8357-846X>

Gerd Ulrich Nienhaus  <https://orcid.org/0000-0002-5027-3192>

References

- [1] Tinnefeld P, Eggeling C and Hell S W (ed) 2015 *Far-Field Optical Nanoscopy*. (Berlin, Heidelberg: Springer)
- [2] Kubitschek U (ed) 2017 *Fluorescence Microscopy: From Principles to Biological Applications*. 2nd ed (Weinheim, Germany: Wiley) p482
- [3] Schermelleh L, Heintzmann R and Leonhardt H 2010 A guide to super-resolution fluorescence microscopy *J. Cell Biol.* **190** 165–75
- [4] Nienhaus K and Nienhaus G U 2016 Where Do We stand with super-resolution optical microscopy? *J. Mol. Biol.* **428** 308–22
- [5] Vangindertael J, Camacho R, Sempels W, Mizuno H, Dedecker P and Janssen K P F 2018 An introduction to optical super-resolution microscopy for the adventurous biologist *Methods. Appl. Fluoresc.* **6** 022003
- [6] Dean K M and Palmer A E 2014 Advances in fluorescence labeling strategies for dynamic cellular imaging *Nat. Chem. Biol.* **10** 512–23
- [7] Jung D, Min K, Jung J, Jang W and Kwon Y 2013 Chemical biology-based approaches on fluorescent labeling of proteins in live cells *Mol. Biosyst.* **9** 862–72
- [8] Nienhaus K and Nienhaus G U 2017 *Fluorescence labeling Fluorescence Microscopy: From Principles to Biological Applications* ed U Kubitschek (Weinheim, Germany: Wiley) pp 143–74
- [9] Chalfie M, Tu Y, Euskirchen G, Ward W W and Prasher D C 1994 Green fluorescent protein as a marker for gene expression *Science* **263** 802–5
- [10] Prasher D C 1995 Using GFP to see the light *Trends Genet.* **11** 320–3
- [11] Nienhaus G U 2008 The green fluorescent protein: a key tool to study chemical processes in living cells *Angew. Chem. Intl. Ed. Engl.* **47** 8992–4
- [12] Jing C and Cornish V W 2011 Chemical Tags for Labeling Proteins Inside Living Cells *Acc. Chem. Res.* **44** 784–92
- [13] Hoelzel C A and Zhang X 2020 Visualizing and manipulating biological processes by using halotag and SNAP-tag technologies *ChemBioChem* **21** 1935–46
- [14] Wilhelm J *et al* 2021 Kinetic and structural characterization of the self-labeling protein tags halotag7, SNAP-tag, and CLIP-tag *Biochemistry* **60** 2560–75
- [15] Paige J S, Wu K Y and Jaffrey S R 2011 RNA mimics of green fluorescent protein *Science* **333** 642–6
- [16] Su Y and Hammond M C 2020 RNA-based fluorescent biosensors for live cell imaging of small molecules and RNAs *Curr. Opin. Biotechnol.* **63** 157–66
- [17] Sunbul M, Lackner J, Martin A, Englert D, Hacene B, Nienhaus K, Nienhaus G U and Jäschke A 2021 Super-resolution RNA imaging using a rhodamine-binding aptamer with fast exchange kinetics *Nat. Biotechnol.* **39** 686–90
- [18] Jung G (ed) 2013 *Fluorescent Proteins I: From Understanding to Design*. (Berlin, Heidelberg: Springer)
- [19] Jung G (ed) 2014 *Fluorescent Proteins II: Application of Fluorescent Protein Technology*. (Berlin, Heidelberg: Springer)
- [20] Shimomura O, Johnson F H and Saiga Y 1962 Extraction, purification and properties of aequorin, a bioluminescent protein from the luminous hydromedusa, *Aequorea J. Cell. Physiol.* **59** 223–39
- [21] Prasher D C, Eckenrode V K, Ward W W, Prendergast F G and Cormier M J 1992 Primary structure of the *Aequorea victoria* green-fluorescent protein *Gene* **111** 229–33
- [22] Tsien R Y 1998 The green fluorescent protein *Annu. Rev. Biochem.* **67** 509–44
- [23] Matz M V, Fradkov A F, Labas Y A, Savitsky A P, Zaraisky A G, Markelov M I and Lukyanov S A 1999 Fluorescent proteins from nonbioluminescent anthozoa species *Nat. Biotechnol.* **17** 969–73
- [24] Wiedenmann J, Elke C, Spindler K D and Funke W 2000 Cracks in the beta-can: fluorescent proteins from *Anemonia sulcata* (Anthozoa, Actinaria) *Proc. Natl. Acad. Sci. USA* **97** 14091–6
- [25] Nienhaus G U and Wiedenmann J 2009 Structure, dynamics and optical properties of fluorescent proteins: perspectives for marker development *ChemPhysChem* **10** 1369–79
- [26] Shaner N C, Steinbach P A and Tsien R Y 2005 A guide to choosing fluorescent proteins *Nat. Methods* **2** 905–9
- [27] Lukyanov K A, Chudakov D M, Lukyanov S and Verkhusha V V 2005 Innovation: Photoactivatable fluorescent proteins *Nat. Rev. Mol. Cell Biol.* **6** 885–91
- [28] Rodriguez E A, Campbell R E, Lin J Y, Lin M Z, Miyawaki A, Palmer A E, Shu X, Zhang J and Tsien R Y 2017 The growing and glowing toolbox of fluorescent and photoactive proteins *Trends Biochem. Sci.* **42** 111–29
- [29] Wiedenmann J, Gayda S, Adam V, Oswald F, Nienhaus K, Bourgeois D and Nienhaus G U 2011 From EosFP to mIrisFP: structure-based development of advanced photoactivatable marker proteins of the GFP-family *J Biophoton.* **4** 377–90

- [30] Lippincott-Schwartz J and Patterson GH 2009 Photoactivatable fluorescent proteins for diffraction-limited and super-resolution imaging *Trends Cell Biol.* **19** 555–65
- [31] Balleza E, Kim J M and Cluzel P 2018 Systematic characterization of maturation time of fluorescent proteins in living cells *Nat. Methods* **15** 47–51
- [32] Craggs T D 2009 Green fluorescent protein: structure, folding and chromophore maturation *Chem. Soc. Rev.* **38** 2865–75
- [33] He X, Bell A F and Tonge P J 2003 Ground state isomerization of a model green fluorescent protein chromophore *FEBS Lett.* **549** 35–8
- [34] Weber W, Helms V, McCammon J A and Langhoff P W 1999 Shedding light on the dark and weakly fluorescent states of green fluorescent proteins *Proc. Natl. Acad. Sci. U S A* **96** 6177–82
- [35] Voityuk A A, Michel-Beyerle M E and Rösch N 1998 Quantum chemical modeling of structure and absorption spectra of the chromophore in green fluorescent proteins *Chem. Phys.* **231** 13–25
- [36] Kummer A D, Kompa C, Niwa H, Hirano T, Kojima S and Michel-Beyerle M E 2002 Viscosity-dependent fluorescence decay of the GFP chromophore in solution due to fast internal conversion *J. Phys. Chem. B* **106** 7554–9
- [37] Wiedenmann J, Schenk A, Röcker C, Girod A, Spindler K D and Nienhaus G U 2002 A far-red fluorescent protein with fast maturation and reduced oligomerization tendency from entacmaea quadricolor (Anthozoa, Actinaria) *Proc. Natl. Acad. Sci. U S A* **99** 11646–51
- [38] Nienhaus K, Nar H, Heilker R, Wiedenmann J and Nienhaus G U 2008 Trans-cis isomerization is responsible for the red-shifted fluorescence in variants of the red fluorescent protein eqFP611 *J. Am. Chem. Soc.* **130** 12578–9
- [39] Kredel S *et al* 2008 Optimized and far-red emitting variants of fluorescent protein eqFP611 *Chem. Biol.* **15** 224–33
- [40] Kredel S, Oswald F, Nienhaus K, Deuschle K, Röcker C, Wolff M, Heilker R, Nienhaus G U and Wiedenmann J 2009 mRuby, a bright monomeric red fluorescent protein for labeling of subcellular structures *PLoS One* **4** e4391
- [41] Wiedenmann J, Vallone B, Renzi F, Nienhaus K, Ivanchenko S, Röcker C and Nienhaus G U 2005 The red fluorescent protein eqFP611 and its genetically engineered dimeric variants *J. Biomed. Opt.* **10** 14003
- [42] Elsiger M A, Wachter R M, Hanson G T, Kallio K and Remington S J 1999 Structural and spectral response of green fluorescent protein variants to changes in pH *Biochemistry* **38** 5296–301
- [43] Chattoraj M, King B A, Bublitz G U and Boxer S G 1996 Ultrafast excited state dynamics in green fluorescent protein: multiple states and proton transfer *Proc. Natl. Acad. Sci. U S A* **93** 8362–7
- [44] Ward W W, Prentice H J, Roth A F, Cody C W and Reeves S C 1982 Spectral perturbations of the *aequorea* green-fluorescent protein *Photochem. Photobiol.* **35** 803–8
- [45] Scharnagl C, Raupp-Kossmann R and Fischer S F 1999 Molecular basis for pH sensitivity and proton transfer in green fluorescent protein: protonation and conformational substates from electrostatic calculations *Biophys. J.* **77** 1839–57
- [46] Bizzarri R *et al* 2007 Green fluorescent protein ground states: the influence of a second protonation site near the chromophore *Biochemistry* **46** 5494–504
- [47] Nienhaus K, Renzi F, Vallone B, Wiedenmann J and Nienhaus G U 2006 Chromophore-protein interactions in the anthozoan green fluorescent protein asFP499 *Biophys. J.* **91** 4210–20
- [48] Nienhaus K, Renzi F, Vallone B, Wiedenmann J and Nienhaus G U 2006 Exploring chromophore-protein interactions in fluorescent protein cmFP512 from *Cerianthus membranaceus*: X-ray structure analysis and optical spectroscopy *Biochemistry* **45** 12942–53
- [49] Gayda S, Nienhaus K and Nienhaus G U 2012 Mechanistic insights into reversible photoactivation in proteins of the GFP family *Biophys. J.* **103** 2521–31
- [50] Loos D C, Habuchi S, Flors C, Hotta J, Wiedenmann J, Nienhaus G U and Hofkens J 2006 Photoconversion in the red fluorescent protein from the sea anemone entacmaea quadricolor: is cis-trans isomerization involved? *J. Am. Chem. Soc.* **128** 6270–1
- [51] Wiedenmann J, Oswald F and Nienhaus G U 2009 Fluorescent proteins for live cell imaging: opportunities, limitations, and challenges *IUBMB Life* **61** 1029–42
- [52] Sniegowski J A, Phail M E and Wachter R M 2005 Maturation efficiency, trypsin sensitivity, and optical properties of Arg96, Glu222, and Gly67 variants of green fluorescent protein *Biochem. Biophys. Res. Commun.* **332** 657–63
- [53] Zacharias D A, Violin J D, Newton A C and Tsien R Y 2002 Partitioning of lipid-modified monomeric GFPs into membrane microdomains of live cells *Science* **296** 913–6
- [54] Wiedenmann J, Ivanchenko S, Oswald F, Schmitt F, Röcker C, Salih A, Spindler K D and Nienhaus G U 2004 EosFP, a fluorescent marker protein with UV-inducible green-to-red fluorescence conversion *Proc. Natl. Acad. Sci. U S A* **101** 15905–10
- [55] Campbell R E, Tour O, Palmer A E, Steinbach P A, Baird G S, Zacharias D A and Tsien R Y 2002 A monomeric red fluorescent protein *Proc. Natl. Acad. Sci. U S A* **99** 7877–82
- [56] Habuchi S, Tsutsui H, Kochaniak A B, Miyawaki A and van Oijen A M 2008 mKikGR, a monomeric photoswitchable fluorescent protein *PLoS One* **3** e3944
- [57] Durisic N, Laparra-Cuervo L, Sandoval-Alvarez A, Borbely J S and Lakadamyali M 2014 Single-molecule evaluation of fluorescent protein photoactivation efficiency using an *in vivo* nanotemplate *Nat. Methods* **11** 156–62
- [58] Ogawa H, Inouye S, Tsuji F I, Yasuda K and Umesono K 1995 Localization, trafficking, and temperature-dependence of the *Aequorea* green fluorescent protein in cultured vertebrate cells *Proc. Natl. Acad. Sci. U S A* **92** 11899–903
- [59] Siemering K R, Golbik R, Sever R and Haseloff J 1996 Mutations that suppress the thermostability of green fluorescent protein *Curr. Biol.* **6** 1653–63
- [60] Dickson R M, Cubitt A B, Tsien R Y and Moerner W E 1997 On/off blinking and switching behaviour of single molecules of green fluorescent protein *Nature* **388** 355–8
- [61] Bogdanov A M, Mishin A S, Yampolsky I V, Belousov V V, Chudakov D M, Subach F V, Verkhusa V V, Lukyanov S and Lukyanov K A 2009 Green fluorescent proteins are light-induced electron donors *Nat. Chem. Biol.* **5** 459–61
- [62] Bosisio C, Quercioli V, Collini M, D'Alfonso L, Baldini G, Bettati S, Campanini B, Raboni S and Chirico G 2008 Protonation and conformational dynamics of GFP mutants by two-photon excitation fluorescence correlation spectroscopy *J. Phys. Chem. B* **112** 8806–14
- [63] Adam V, Carpentier P, Violot S, Lelimosin M, Darnault C, Nienhaus G U and Bourgeois D 2009 Structural basis of X-ray-induced transient photobleaching in a photoactivatable green fluorescent protein *J. Am. Chem. Soc.* **131** 18063–5
- [64] Haupts U, Maiti S, Schulle P and Webb W W 1998 Dynamics of fluorescence fluctuations in green fluorescent protein observed by fluorescence correlation spectroscopy *Proc. Natl. Acad. Sci. U S A* **95** 13573–8
- [65] Hendrix J, Flors C, Dedecker P, Hofkens J and Engelborghs Y 2008 Dark states in monomeric red fluorescent proteins studied by fluorescence correlation and single molecule spectroscopy *Biophys. J.* **94** 4103–13
- [66] Schenk A, Ivanchenko S, Röcker C, Wiedenmann J and Nienhaus G U 2004 Photodynamics of red fluorescent proteins studied by fluorescence correlation spectroscopy *Biophys. J.* **86** 384–94
- [67] Bogdanov A M, Acharya A, Titelmayer A V, Mamontova A V, Bravaya K B, Kolomeisky A B, Lukyanov K A and Krylov A I 2016 Turning on and off photoinduced electron transfer in fluorescent proteins by pi-stacking, halide binding, and Tyr145 mutations *J. Am. Chem. Soc.* **138** 4807–17
- [68] Roy A, Field M J, Adam V and Bourgeois D 2011 The nature of transient dark states in a photoactivatable fluorescent protein *J. Am. Chem. Soc.* **133** 18586–9
- [69] Duan C, Adam V, Byrdin M, Ridard J, Kieffer-Jaquinod S, Morlot C, Arcizet D, Demachy I and Bourgeois D 2013

- Structural evidence for a two-regime photobleaching mechanism in a reversibly switchable fluorescent protein *J. Am. Chem. Soc.* **135** 15841–50
- [70] Vegh R B, Bravaya K B, Bloch D A, Bommarius A S, Tolbert L M, Verkhovskiy M, Krylov A I and Solntsev K M 2014 Chromophore photoreduction in red fluorescent proteins is responsible for bleaching and phototoxicity *J. Phys. Chem. B* **118** 4527–34
- [71] Bindels D S *et al* 2017 Mscarlet: a bright monomeric red fluorescent protein for cellular imaging *Nat. Methods* **14** 53–6
- [72] Costantini L M and Snapp E L 2013 Fluorescent proteins in cellular organelles: serious pitfalls and some solutions *DNA Cell Biol.* **32** 622–7
- [73] Costantini L M, Baloban M, Markwardt M L, Rizzo M, Guo F, Verkhusha V V and Snapp E L 2015 A palette of fluorescent proteins optimized for diverse cellular environments *Nat. Commun.* **6** 7670
- [74] Remington S J 2006 Fluorescent proteins: maturation, photochemistry and photophysics *Curr. Opin. Struct. Biol.* **16** 714–21
- [75] Bulina M E *et al* 2006 A genetically encoded photosensitizer *Nat. Biotechnol.* **24** 95–9
- [76] Takemoto K *et al* 2013 SuperNova, a monomeric photosensitizing fluorescent protein for chromophore-assisted light inactivation *Sci Rep.* **3** 2629
- [77] Lambert T J 2019 FPbase: a community-editable fluorescent protein database *Nat. Methods* **16** 277–8
- [78] Zhang M *et al* 2012 Rational design of true monomeric and bright photoactivatable fluorescent proteins *Nat. Methods* **9** 727–9
- [79] Adam V *et al* 2011 Rational design of photoconvertible and biphotochromic fluorescent proteins for advanced microscopy applications *Chem. Biol.* **18** 1241–51
- [80] Nienhaus K and Nienhaus G U 2016 Chromophore photophysics and dynamics in fluorescent proteins of the GFP family *J. Phys. Condens. Matter* **28** 443001
- [81] Tsien R Y, Ernst L and Waggoner A 2006 Fluorophores for confocal microscopy: photophysics and photochemistry *Handbook Of Biological Confocal Microscopy* ed J B Pawley (US, Boston, MA: Springer) 338–52
- [82] Ha T and Tinnefeld P 2012 Photophysics of fluorescent probes for single-molecule biophysics and super-resolution imaging *Annu. Rev. Phys. Chem.* **63** 595–617
- [83] Heim R, Prasher D C and Tsien R Y 1994 Wavelength mutations and posttranslational autoxidation of green fluorescent protein *Proc. Natl. Acad. Sci. U S A* **91** 12501–4
- [84] Lossau H *et al* 1996 Time-resolved spectroscopy of wild-type and mutant green fluorescent proteins reveals excited state deprotonation consistent with fluorophore-protein interactions *Chem. Phys.* **213** 1–16
- [85] Piatkevich K D, Hulit J, Subach O M, Wu B, Abdulla A, Segall J E and Verkhusha V V 2010 Monomeric red fluorescent proteins with a large Stokes shift *Proc. Natl. Acad. Sci. U S A* **107** 5369–74
- [86] Piatkevich K D, Malashkevich V N, Almo S C and Verkhusha V V 2010 Engineering ESPT pathways based on structural analysis of LSSmKate red fluorescent proteins with large Stokes shift *J. Am. Chem. Soc.* **132** 10762–70
- [87] Subach O M *et al* 2021 LSSmScarlet, dCyRFP2s, dCyOFF2s and CRISPRed2s, Genetically Encoded Red Fluorescent Proteins with a Large Stokes Shift *Int. J. Mol. Sci.* **22** 12887
- [88] Yang J, Wang L, Yang F, Luo H, Xu L, Lu J, Zeng S and Zhang Z 2013 Mberfp, an improved large Stokes shift red fluorescent protein *PLoS One* **8** e64849
- [89] Brakemann T *et al* 2011 A reversibly photoswitchable GFP-like protein with fluorescence excitation decoupled from switching *Nat. Biotechnol.* **29** 942–7
- [90] Arai Y, Takauchi H, Ogami Y, Fujiwara S, Nakano M, Matsuda T and Nagai T 2018 Spontaneously blinking fluorescent protein for simple single laser super-resolution live cell imaging *ACS Chem. Biol.* **13** 1938–43
- [91] Nienhaus K and Nienhaus G U 2014 Fluorescent proteins for live-cell imaging with super-resolution *Chem. Soc. Rev.* **43** 1088–106
- [92] Stiel A C *et al* 2008 Generation of monomeric reversibly switchable red fluorescent proteins for far-field fluorescence nanoscopy *Biophys. J.* **95** 2989–97
- [93] Shinoda H, Lu K, Nakashima R, Wazawa T, Noguchi K, Matsuda T and Nagai T 2019 Acid-tolerant reversibly switchable green fluorescent protein for super-resolution imaging under acidic conditions *Cell Chem. Biol.* **26** 1469–79.e06
- [94] van Thor J J, Gensch T, Hellingwerf K J and Johnson L N 2002 Phototransformation of green fluorescent protein with UV and visible light leads to decarboxylation of glutamate 222 *Nat. Struct. Biol.* **9** 37–41
- [95] Patterson G H and Lippincott-Schwartz J 2002 A photoactivatable GFP for selective photolabeling of proteins and cells *Science* **297** 1873–7
- [96] Henderson J N, Gepshtein R, Heenan J R, Kallio K, Huppert D and Remington S J 2009 Structure and mechanism of the photoactivatable green fluorescent protein *J. Am. Chem. Soc.* **131** 4176–7
- [97] Gurskaya N G, Verkhusha V V, Shcheglov A S, Staroverov D B, Chepurnykh T V, Fradkov A F, Lukyanov S and Lukyanov K A 2006 Engineering of a monomeric green-to-red photoactivatable fluorescent protein induced by blue light *Nat. Biotechnol.* **24** 461–5
- [98] Thedie D, Berardozi R, Adam V and Bourgeois D 2017 Photoswitching of green mEos2 by intense 561 nm light perturbs efficient green-to-red photoconversion in localization microscopy *J. Phys. Chem. Lett.* **8** 4424–30
- [99] Makarov N S, Cirloganu C, Perry J W, Lukyanov K A and Solntsev K M 2014 Steady-state and time-resolved spectroscopic studies of green-to-red photoconversion of fluorescent protein Dendra2 *J. Photochem. Photobiol. A* **280** 5–13
- [100] Klementieva N V, Lukyanov K A, Markina N M, Lukyanov S A, Zagaynova E V and Mishin A S 2016 Green-to-red primed conversion of Dendra2 using blue and red lasers *Chem. Commun.* **52** 13144–6
- [101] Mohr M A, Kobitski A Y, Sabater L R, Nienhaus K, Obara C J, Lippincott-Schwartz J, Nienhaus G U and Pantazis P 2017 Rational engineering of photoconvertible fluorescent proteins for dual-color fluorescence nanoscopy enabled by a triplet-state mechanism of primed conversion *Angew. Chem. Int. Ed. Engl.* **56** 11628–33
- [102] Turkowyd B, Balinovic A, Virant D, Carnero H G G, Caldana F, Endesfelder M, Bourgeois D and Endesfelder U 2017 A general mechanism of photoconversion of green-to-red fluorescent proteins based on blue and infrared light reduces phototoxicity in live-cell single-molecule imaging *Angew. Chem. Int. Ed. Engl.* **56** 11634–9
- [103] Adam V *et al* 2008 Structural characterization of IrisFP, an optical highlighter undergoing multiple photo-induced transformations *Proc. Natl. Acad. Sci. U S A* **105** 18343–8
- [104] Fuchs J, Böhme S, Oswald F, Hedde P N, Krause M, Wiedenmann J and Nienhaus G U 2010 A photoactivatable marker protein for pulse-chase imaging with superresolution *Nat. Methods* **7** 627–30
- [105] Oliinyk O S, Chernov K G and Verkhusha V V 2017 Bacterial phytochromes, cyanobacteriochromes and allophycocyanins as a source of near-infrared fluorescent probes *Int. J. Mol. Sci.* **18** 1691
- [106] Toh K C, Stojković E A, van Stokkum I H M, Moffat K and Kennis J T M 2010 Proton-transfer and hydrogen-bond interactions determine fluorescence quantum yield and photochemical efficiency of bacteriophytochrome *Proc. Natl. Acad. Sci. U S A* **107** 9170–5
- [107] Samma A A, Johnson C K, Song S, Alvarez S and Zimmer M 2010 On the origin of fluorescence in bacteriophytochrome infrared fluorescent proteins *J. Phys. Chem. B* **114** 15362–9

- [108] Montecinos-Franjola F, Lin J Y and Rodriguez E A 2020 Fluorescent proteins for *in vivo* imaging, where's the biliverdin? *Biochem. Soc. Trans.* **48** 2657–67
- [109] Hayashi S and Toda Y 2009 A novel fluorescent protein purified from eel muscle *Fish. Sci.* **75** 1461–9
- [110] Kumagai A, Ando R, Miyatake H, Greimel P, Kobayashi T, Hirabayashi Y, Shimogori T and Miyawaki A 2013 A bilirubin-inducible fluorescent protein from eel muscle *Cell* **153** 1602–11
- [111] Guarnaccia A M, Krivoschik S R, Sparks J S, Gruber D F and Gaffney J P 2021 Discovery and characterization of a bilirubin inducible green fluorescent protein from the moray eel *gymnothorax zonipectis* *Front. Mar. Sci.* **8** 678571
- [112] Gruber D F, Gaffney J P, Mehr S, DeSalle R, Sparks J S, Platasa J and Pieribone V A 2015 Adaptive evolution of eel fluorescent proteins from fatty acid binding proteins produces bright fluorescence in the marine environment *PLoS One* **10** e0140972
- [113] Krivoschik S R, Guarnaccia A M, Fried D B, Gruber D F and Gaffney J P 2020 Disrupting fluorescence by mutagenesis in a green fluorescent fatty acid binding protein from a marine eel *Protein J.* **39** 145–51
- [114] Kwon J *et al* 2020 Bright ligand-activatable fluorescent protein for high-quality multicolor live-cell super-resolution microscopy *Nat. Commun.* **11** 273
- [115] Yeh J T, Nam K, Yeh J T and Perrimon N 2017 eUnaG: a new ligand-inducible fluorescent reporter to detect drug transporter activity in live cells *Sci Rep.* **7** 41619
- [116] Park J S, Nam E, Lee H K, Lim M H and Rhee H W 2016 In Cellulo Mapping of Subcellular Localized Bilirubin *ACS Chem. Biol.* **11** 2177–85
- [117] To T L, Zhang Q, Shu X 2016 Structure-guided design of a reversible fluorogenic reporter of protein-protein interactions *Protein Sci.* **25** 748–53
- [118] Rodriguez E A, Tran G N, Gross L A, Crisp J L, Shu X, Lin J Y and Tsien R Y 2016 A far-red fluorescent protein evolved from a cyanobacterial phycobiliprotein *Nat. Methods* **13** 763–9
- [119] Ding W L, Miao D, Hou Y N, Jiang S P, Zhao B Q, Zhou M, Scheer H and Zhao K H 2017 Small monomeric and highly stable near-infrared fluorescent markers derived from the thermophilic phycobiliprotein *ApcF2* *Biochim. Biophys. Acta Mol. Cell Res.* **1864** 1877–86
- [120] Machado J-H, Ting R, Lin J Y and Rodriguez E A 2021 A self-labeling protein based on the small ultra-red fluorescent protein, smURFP *RSC Chem. Biol.* **2** 1221–6
- [121] Sharrock R A 2008 The phytochrome red/far-red photoreceptor superfamily *Genome Biol.* **9** 230
- [122] Davis S J, Vener A V and Vierstra R D 1999 Bacteriophytochromes: phytochrome-like photoreceptors from nonphotosynthetic eubacteria *Science* **286** 2517–20
- [123] Shcherbakova D M, Baloban M and Verkhusha V V 2015 Near-infrared fluorescent proteins engineered from bacterial phytochromes *Curr. Opin. Chem. Biol.* **27** 52–63
- [124] Shu X, Royant A, Lin M Z, Aguilera T A, Lev-Ram V, Steinbach P A and Tsien R Y 2009 Mammalian expression of infrared fluorescent proteins engineered from a bacterial phytochrome *Science* **324** 804–7
- [125] Shcherbakova D M and Verkhusha V V 2013 Near-infrared fluorescent proteins for multicolor *in vivo* imaging *Nat. Methods* **10** 751–4
- [126] Yu D *et al* 2014 An improved monomeric infrared fluorescent protein for neuronal and tumour brain imaging *Nat. Commun.* **5** 1–7
- [127] Bhattacharya S, Auldridge M E, Lehtivuori H, Ihalainen J A and Forest K T 2014 Origins of fluorescence in evolved bacteriophytochromes *J. Biol. Chem.* **289** 32144–52
- [128] Auldridge M E, Satyshur K A, Anstrom D M and Forest K T 2012 Structure-guided engineering enhances a phytochrome-based infrared fluorescent protein *J. Biol. Chem.* **287** 7000–9
- [129] Filonov G S, Piatkevich K D, Ting L-M, Zhang J, Kim K and Verkhusha V V 2011 Bright and stable near-infrared fluorescent protein for *in vivo* imaging *Nat. Biotechnol.* **29** 757–61
- [130] Bansal S, Biswas G and Avadhani N G 2014 Mitochondria-targeted heme oxygenase-1 induces oxidative stress and mitochondrial dysfunction in macrophages, kidney fibroblasts and in chronic alcohol hepatotoxicity *Redox Biol.* **2** 273–83
- [131] Matlashov M E, Shcherbakova D M, Alvelid J, Baloban M, Pennacchietti F, Shemetov A A, Testa I and Verkhusha V V 2020 A set of monomeric near-infrared fluorescent proteins for multicolor imaging across scales *Nat. Commun.* **11** 239
- [132] Piatkevich K D, Subach F V and Verkhusha V V 2013 Far-red light photoactivatable near-infrared fluorescent proteins engineered from a bacterial phytochrome *Nat. Commun.* **4** 2153
- [133] Fushimi K and Narikawa R 2019 Cyanobacteriochromes: photoreceptors covering the entire UV-to-visible spectrum *Curr. Opin. Struct. Biol.* **57** 39–46
- [134] Oliinyk O S, Shemetov A A, Pletnev S, Shcherbakova D M and Verkhusha V V 2019 Smallest near-infrared fluorescent protein evolved from cyanobacteriochrome as versatile tag for spectral multiplexing *Nat. Commun.* **10** 279
- [135] Zhang J, Wu X-J, Wang Z-B, Chen Y, Wang X, Zhou M, Scheer H and Zhao K-H 2010 Fused-gene approach to photoswitchable and fluorescent biliproteins *Angew. Chem. Int. Ed.* **49** 5456–8
- [136] Sanderson M J, Smith I, Parker I and Bootman M D 2014 Fluorescence microscopy *Cold Spring Harbor Protocols* **2014**
- [137] Lichtman J W and Conchello J A 2005 Fluorescence microscopy *Nat. Methods* **2** 910–9
- [138] Pawley James B. (ed) 2006 *Handbook of Biological Confocal Microscopy*. (Boston, MA: Springer)
- [139] Baddeley D and Bewersdorf J 2018 Biological insight from super-resolution microscopy: what we can learn from localization-based images *Annu. Rev. Biochem.* **87** 965–89
- [140] Lelek M *et al* 2021 Single-molecule localization microscopy *Nat. Rev. Methods Primers* **1** 39
- [141] Valli J, Garcia-Burgos A, Rooney L M, Vale de Melo E O B, Duncan R R and Rickman C 2021 Seeing beyond the limit: a guide to choosing the right super-resolution microscopy technique *J. Biol. Chem.* **297** 100791
- [142] Jonkman J, Brown C M, Wright G D, Anderson K I and North A J 2020 Tutorial: guidance for quantitative confocal microscopy *Nat. Protoc.* **15** 1585–611
- [143] Conchello J-A and Lichtman J W 2005 Optical sectioning microscopy *Nat. Methods* **2** 920–31
- [144] Gong W, Das P, Samanta S, Xiong J, Pan W, Gu Z, Zhang J, Qu J and Yang Z 2019 Redefining the photo-stability of common fluorophores with triplet state quenchers: mechanistic insights and recent updates *Chem. Commun.* **55** 8695–704
- [145] Nemet I, Ropelewski P and Imanishi Y 2015 Applications of phototransformable fluorescent proteins for tracking the dynamics of cellular components *Photochem. Photobiol. Sci.* **14** 1787–806
- [146] Chung K *et al* 2013 Structural and molecular interrogation of intact biological systems *Nature* **497** 332–7
- [147] Scott D J *et al* 2018 A novel ultra-stable, monomeric green fluorescent protein for direct volumetric imaging of whole organs using CLARITY *Sci Rep.* **8** 667
- [148] Hell S W 2009 Microscopy and its focal switch *Nat. Methods* **6** 24–32
- [149] Morozova K S, Piatkevich K D, Gould T J, Zhang J, Bewersdorf J and Verkhusha V V 2010 Far-red fluorescent protein excitable with red lasers for flow cytometry and superresolution STED nanoscopy *Biophys. J.* **99** L13–5
- [150] Strack R L, Hein B, Bhattacharyya D, Hell S W, Keenan R J and Glick B S 2009 A rapidly maturing far-red derivative of dsred-express2 for whole-cell labeling *Biochemistry* **48** 8279–81
- [151] Matela G, Gao P, Guigas G, Eckert A F, Nienhaus K and Nienhaus G U 2017 A far-red emitting fluorescent marker

- protein, mGarnet2, for microscopy and STED nanoscopy *Chem. Commun.* **53** 979–82
- [152] Hense A, Prunsche B, Gao P, Ishitsuka Y, Nienhaus K and Nienhaus G U 2015 Monomeric Garnet, a far-red fluorescent protein for live-cell STED imaging *Sci Rep.* **5** 18006
- [153] Wegner W, Ilgen P, Gregor C, van Dort J, Mott A C, Steffens H and Willig K I 2017 *in vivo* mouse and live cell STED microscopy of neuronal actin plasticity using far-red emitting fluorescent proteins *Sci Rep.* **7** 11781
- [154] Gao P, Prunsche B, Zhou L, Nienhaus K and Nienhaus G U 2017 Background suppression in fluorescence nanoscopy with stimulated emission double depletion *Nat. Photon.* **11** 163–9
- [155] Kamper M, Ta H, Jensen N A, Hell S W and Jakobs S 2018 Near-infrared STED nanoscopy with an engineered bacterial phytochrome *Nat. Commun.* **9** 4762
- [156] Hell S W and Kroug M 1995 Ground-state depletion fluorescence microscopy, a concept for breaking the diffraction resolution limit *Appl. Phys. B* **60** 495–7
- [157] Bretschneider S, Eggeling C and Hell S W 2007 Breaking the diffraction barrier in fluorescence microscopy by optical shelving *Phys. Rev. Lett.* **98** 218103
- [158] Bossi M, Fölling J, Dyba M, Westphal V and Hell S W 2006 Breaking the diffraction resolution barrier in far-field microscopy by molecular optical bistability *New J. Phys.* **8** 275
- [159] Hofmann M, Eggeling C, Jakobs S and Hell S W 2005 Breaking the diffraction barrier in fluorescence microscopy at low light intensities by using reversibly photoswitchable proteins *Proc. Natl. Acad. Sci. U S A* **102** 17565–9
- [160] Hell S W 2005 Fluorescence nanoscopy: breaking the diffraction barrier by the RESOLFT concept *NanoBiotechnology* **1** 296–7
- [161] Dedecker P *et al* 2007 Subdiffraction imaging through the selective donut-mode depletion of thermally stable photoswitchable fluorophores: numerical analysis and application to the fluorescent protein dronpa *J. Am. Chem. Soc.* **129** 16132–41
- [162] Chang H *et al* 2012 A unique series of reversibly switchable fluorescent proteins with beneficial properties for various applications *Proc. Natl. Acad. Sci. U S A* **109** 4455–60
- [163] Nienhaus G U 2012 A fatigue-resistant photoswitchable fluorescent protein for optical nanoscopy *Angew. Chem. Int. Ed. Engl.* **51** 1312–4
- [164] Grotjohann T, Testa I, Reuss M, Brakemann T, Eggeling C, Hell S W and Jakobs S 2012 rsEGFP2 enables fast RESOLFT nanoscopy of living cells *eLife* **1** e00248
- [165] Konen T, Stumpf D, Grotjohann T, Jansen I, Bossi M, Weber M, Jensen N, Hell S W and Jakobs S 2021 The positive switching fluorescent protein padron2 enables live-cell reversible saturable optical linear fluorescence transitions (RESOLFT) nanoscopy without sequential illumination steps *ACS Nano* **15** 9509–21
- [166] Testa I, D'Este E, Urban N T, Balzarotti F and Hell S W 2015 Dual channel RESOLFT nanoscopy by using fluorescent state kinetics *Nano Lett.* **15** 103–6
- [167] Ilgen P, Grotjohann T, Jans D C, Kilisch M, Hell S W and Jakobs S 2015 RESOLFT nanoscopy of fixed cells using a z-domain based fusion protein for labelling *PLoS One* **10** e0136233
- [168] Wang S, Chen X, Chang L, Xue R, Duan H and Sun Y 2016 GMars-q enables long-term live-cell parallelized reversible saturable optical fluorescence transitions nanoscopy *ACS Nano* **10** 9136–44
- [169] Wang S, Shuai Y, Sun C, Xue B, Hou Y, Su X and Sun Y 2018 Lighting up live cells with smart genetically encoded fluorescence probes from gmars family *ACS Sens.* **3** 2269–77
- [170] Nienhaus K and Nienhaus G U 2016 Photoswitchable fluorescent proteins: do not always look on the bright side *ACS Nano* **10** 9104–8
- [171] Subach F V, Zhang L, Gadella T W, Gurskaya N G, Lukyanov K A and Verkhusha V V 2010 Red fluorescent protein with reversibly photoswitchable absorbance for photochromic FRET *Chem. Biol.* **17** 745–55
- [172] Lavoie-Cardinal F, Jensen N A, Westphal V, Stiel A C, Chmyrov A, Bierwagen J, Testa I, Jakobs S and Hell S W 2014 Two-Color RESOLFT Nanoscopy with Green and Red Fluorescent Photochromic Proteins *ChemPhysChem* **15** 655–63
- [173] Pennacchietti F *et al* 2018 Fast reversibly photoswitching red fluorescent proteins for live-cell RESOLFT nanoscopy *Nat. Methods* **15** 601–4
- [174] Masullo L A, Bodén A, Pennacchietti F, Coceano G, Ratz M and Testa I 2018 Enhanced photon collection enables four dimensional fluorescence nanoscopy of living systems *Nat. Commun.* **9** 3281
- [175] Gustafsson M G 2000 Surpassing the lateral resolution limit by a factor of two using structured illumination microscopy *J. Microsc.* **198** 82–7
- [176] Li D *et al* 2015 Extended-resolution structured illumination imaging of endocytic and cytoskeletal dynamics *Science* **349** aab3500
- [177] Wu Y and Shroff H 2018 Faster, sharper, and deeper: structured illumination microscopy for biological imaging *Nat. Methods* **15** 1011–9
- [178] Kner P, Chhun B B, Griffis E R, Winoto L and Gustafsson M G 2009 Super-resolution video microscopy of live cells by structured illumination *Nat. Methods* **6** 339–42
- [179] Gustafsson M G 2005 Nonlinear structured-illumination microscopy: wide-field fluorescence imaging with theoretically unlimited resolution *Proc. Natl. Acad. Sci. U S A* **102** 13081–6
- [180] Heintzmann R and Gustafsson M G 2009 Subdiffraction resolution in continuous samples *Nat. Photon.* **3** 362–4
- [181] Rego E H, Shao L, Macklin J J, Winoto L, Johansson G A, Kamps-Hughes N, Davidson M W and Gustafsson M G 2012 Nonlinear structured-illumination microscopy with a photoswitchable protein reveals cellular structures at 50-nm resolution *Proc. Natl. Acad. Sci. U S A* **109** E135–43
- [182] Heintzmann R, Jovin T M and Cremer C 2002 Saturated patterned excitation microscopy—a concept for optical resolution improvement *J. Opt. Soc. Am.* **19** 1599–609
- [183] Heintzmann R and Huser T 2017 Super-resolution structured illumination microscopy *Chem. Rev.* **117** 13890–908
- [184] Zhang X, Zhang M, Li D, He W, Peng J, Betzig E and Xu P 2016 Highly photostable, reversibly photoswitchable fluorescent protein with high contrast ratio for live-cell superresolution microscopy *Proc. Natl. Acad. Sci. U S A* **113** 10364–9
- [185] Hess S T, Girirajan T P and Mason M D 2006 Ultra-high resolution imaging by fluorescence photoactivation localization microscopy *Biophys. J.* **91** 4258–72
- [186] Betzig E, Patterson G H, Sougrat R, Lindwasser O W, Olenych S, Bonifacino J S, Davidson M W, Lippincott-Schwartz J and Hess H F 2006 Imaging intracellular fluorescent proteins at nanometer resolution *Science* **313** 1642–5
- [187] Rust M J, Bates M and Zhuang X 2006 Sub-diffraction-limit imaging by stochastic optical reconstruction microscopy (STORM) *Nat. Methods* **3** 793–5
- [188] Heilemann M, van de Linde S, Schüttelz M, Kasper R, Seefeldt B, Mukherjee A, Tinnefeld P and Sauer M 2008 Subdiffraction-resolution fluorescence imaging with conventional fluorescent probes *Angew. Chem. Int. Ed. Engl.* **47** 6172–6
- [189] Sharonov A and Hochstrasser R M 2006 Wide-field subdiffraction imaging by accumulated binding of diffusing probes *Proc. Natl. Acad. Sci. U S A* **103** 18911–6
- [190] Giannone G *et al* 2010 Dynamic superresolution imaging of endogenous proteins on living cells at ultra-high density *Biophys. J.* **99** 1303–10
- [191] Schnitzbauer J, Strauss M T, Schlichthaele T, Schueder F and Jungmann R 2017 Super-resolution microscopy with DNA-PAINT *Nat. Protoc.* **12** 1198–228

- [192] Finan K, Flottmann B and Heilemann M 2013 Photoswitchable fluorophores for single-molecule localization microscopy *Methods Mol. Biol.* **950** 131–51
- [193] Mizuno H, Dedecker P, Ando R, Fukano T, Hofkens J and Miyawaki A 2010 Higher resolution in localization microscopy by slower switching of a photochromic protein *Photochem. Photobiol. I Sci.* **9** 239–48
- [194] Lee S H, Shin J Y, Lee A and Bustamante C 2012 Counting single photoactivatable fluorescent molecules by photoactivated localization microscopy (PALM) *Proc. Natl. Acad. Sci. U S A* **109** 17436–41
- [195] Nienhaus K and Nienhaus G U 2021 Fluorescent proteins of the EosFP clade: intriguing marker tools with multiple photoactivation modes for advanced microscopy *RSC Chem. Biol.* **2** 796–814
- [196] Annibale P, Scarselli M, Kodiyan A and Radenovic A 2010 Photoactivatable fluorescent protein mEos2 displays repeated photoactivation after a long-lived dark state in the red photoconverted form *J. Phys. Chem. Lett.* **1** 1506–10
- [197] Annibale P, Vanni S, Scarselli M, Rothlisberger U and Radenovic A 2011 Identification of clustering artifacts in photoactivated localization microscopy *Nat. Methods* **8** 527–8
- [198] Zhou L, Evangelinos M, Wernet V, Eckert A F, Ishitsuka Y, Fischer R, Nienhaus G U and Takeshita N 2018 Superresolution and pulse-chase imaging reveal the role of vesicle transport in polar growth of fungal cells *Sci. Adv.* **4** e1701798
- [199] Wang S, Moffitt J R, Dempsey G T, Xie X S and Zhuang X 2014 Characterization and development of photoactivatable fluorescent proteins for single-molecule-based superresolution imaging *Proc. Natl. Acad. Sci. U S A* **111** 8452–7
- [200] Dempsey G T, Vaughan J C, Chen K H, Bates M and Zhuang X 2011 Evaluation of fluorophores for optimal performance in localization-based super-resolution imaging *Nat. Methods* **8** 1027–36
- [201] Siedentopf H and Zsigmondy R 1902 Über sichtbarmachung und Größenbestimmung ultramikroskopischer Teilchen, mit besonderer anwendung auf goldrubingläser *Ann. Phys.* **315** 1–39
- [202] Girkin J M and Carvalho M T 2018 The light-sheet microscopy revolution *J. Opt.* **20** 053002
- [203] Huisken J, Swoger J, Del Bene F, Wittbrodt J and Stelzer E H 2004 Optical sectioning deep inside live embryos by selective plane illumination microscopy *Science* **305** 1007–9
- [204] Planchon T A, Gao L, Milkie D E, Davidson M W, Galbraith J A, Galbraith C G and Betzig E 2011 Rapid three-dimensional isotropic imaging of living cells using Bessel beam plane illumination *Nat. Methods* **8** 417–23
- [205] Chen B C *et al* 2014 Lattice light-sheet microscopy: Imaging molecules to embryos at high spatiotemporal resolution *Science* **346** 1257998
- [206] Fahrback F O and Rohrbach A 2010 A line scanned light-sheet microscope with phase shaped self-reconstructing beams *Opt. Express* **18** 24229–44
- [207] Vettenburg T, Dalgarno H I C, Nylk J, Coll-Lladó C, Ferrier D E K, Čížmár T, Gunn-Moore F J and Dholakia K 2014 Light-sheet microscopy using an Airy beam *Nat. Methods* **11** 541–4
- [208] Hüpfel M, Fernández Merino M, Bennemann J, Takamiya M, Rastegar S, Tursch A, Holstein T W and Nienhaus G U 2022 Two plus one is almost three: a fast approximation for multi-view deconvolution *Biomed. Opt. Express* **13** 147–58
- [209] Stelzer E H 2015 Light-sheet fluorescence microscopy for quantitative biology *Nat. Methods* **12** 23–6
- [210] Follain G, Mercier L, Osmani N, Harlepp S and Goetz J G 2017 Seeing is believing – multi-scale spatio-temporal imaging towards in vivo cell biology *J. Cell Sci.* **130** 23–38
- [211] Weber M and Huisken J 2011 Light sheet microscopy for real-time developmental biology *Curr. Opin. Genet. Dev.* **21** 566–72
- [212] Berthet B and Maizel A 2016 Light sheet microscopy and live imaging of plants *J. Microsc.* **263** 158–64
- [213] Royer L A, Lemon W C, Chhetri R K, Wan Y, Coleman M, Myers E W and Keller P J 2016 Adaptive light-sheet microscopy for long-term, high-resolution imaging in living organisms *Nat. Biotechnol.* **34** 1267–78
- [214] Weger M *et al* 2020 MondoA regulates gene expression in cholesterol biosynthesis-associated pathways required for zebrafish epiboly *eLife* **9** e57068
- [215] Kobitski A Y *et al* 2015 An ensemble-averaged, cell density-based digital model of zebrafish embryo development derived from light-sheet microscopy data with single-cell resolution *Sci Rep.* **5** 8601
- [216] Mickoleit M, Schmid B, Weber M, Fahrback F O, Hombach S, Reischauer S and Huisken J 2014 High-resolution reconstruction of the beating zebrafish heart *Nat. Methods* **11** 919–22
- [217] Takamiya M *et al* 2020 Pax6 organizes the anterior eye segment by guiding two distinct neural crest waves *PLoS Genet.* **16** e1008774
- [218] Dertinger T, Colyer R, Iyer G, Weiss S and Enderlein J 2009 Fast, background-free, 3D super-resolution optical fluctuation imaging (SOFI) *Proc. Natl. Acad. Sci. U S A* **106** 22287–92
- [219] Dertinger T, Colyer R, Vogel R, Enderlein J and Weiss S 2010 Achieving increased resolution and more pixels with Superresolution Optical Fluctuation Imaging (SOFI) *Opt. Express* **18** 18875–85
- [220] Geissbuehler S, Dellagiocoma C and Lasser T 2011 Comparison between SOFI and STORM *Biomed. Opt. Express* **2** 408–20
- [221] Klementieva N V, Pavlikov A I, Moiseev A A, Bozhanova N G, Mishina N M, Lukyanov S A, Zagaynova E V, Lukyanov K A and Mishin A S 2017 Intrinsic blinking of red fluorescent proteins for super-resolution microscopy *Chem. Commun.* **53** 949–51
- [222] Dedecker P, Mo G C H, Dertinger T and Zhang J 2012 Widely accessible method for superresolution fluorescence imaging of living systems *Proc. Natl. Acad. Sci. U S A* **109** 10909
- [223] Zhang X, Chen X, Zeng Z, Zhang M, Sun Y, Xi P, Peng J and Xu P 2015 Development of a reversibly switchable fluorescent protein for super-resolution optical fluctuation imaging (SOFI) *ACS Nano* **9** 2659–67
- [224] Ando R, Mizuno H and Miyawaki A 2004 Regulated fast nucleocytoplasmic shuttling observed by reversible protein highlighting *Science* **306** 1370–3
- [225] Dertinger T, Pallaoro A, Braun G, Ly S, Laurence T A and Weiss S 2013 Advances in superresolution optical fluctuation imaging (SOFI) *Q. Rev. Biophys.* **46** 210–21
- [226] Mo G C *et al* 2017 Genetically encoded biosensors for visualizing live-cell biochemical activity at super-resolution *Nat. Methods* **14** 427–34
- [227] Lin W, Mo G C H, Mehta S and Zhang J 2021 DrFLINC contextualizes super-resolution activity imaging *J. Am. Chem. Soc.* **143** 14951–5
- [228] Ando T *et al* 2018 The 2018 correlative microscopy techniques roadmap *J. Phys. D: Appl. Phys.* **51** 443001
- [229] Hauser M, Wojcik M, Kim D, Mahmoudi M, Li W and Xu K 2017 Correlative super-resolution microscopy: new dimensions and new opportunities *Chem. Rev.* **117** 7428–56
- [230] Li Y, Shang L and Nienhaus G U 2016 Super-resolution imaging-based single particle tracking reveals dynamics of nanoparticle internalization by live cells *Nanoscale* **8** 7423–9
- [231] Zhou L, Obhof T, Schneider K, Feldbrugge M, Nienhaus G U and Kamper J 2018 Cytoplasmic Transport Machinery of the SPF27 Homologue Num1 in *Ustilago maydis* *Sci Rep.* **8** 3611
- [232] Odermatt P D, Shivanandan A, Deschout H, Jankele R, Nievergelt A P, Feletti L, Davidson M W, Radenovic A and Fantner G E 2015 High-resolution correlative microscopy: bridging the gap between single molecule localization microscopy and atomic force microscopy *Nano Lett.* **15** 4896–904
- [233] Gómez-Varela A I, Stavov D R, Miranda A, Alves R, Barata-Antunes C, Dambournet D, Drubin D G, Paiva S,

- De and Beule P A A 2020 Simultaneous co-localized super-resolution fluorescence microscopy and atomic force microscopy: combined SIM and AFM platform for the life sciences *Sci Rep.* **10** 1122
- [234] Navikas V *et al* 2021 Correlative 3D microscopy of single cells using super-resolution and scanning ion-conductance microscopy *Nat. Commun.* **12** 4565
- [235] Inavalli V V G K *et al* 2019 A super-resolution platform for correlative live single-molecule imaging and STED microscopy *Nat. Methods* **16** 1263–8
- [236] Tanida I, Furuta Y, Yamaguchi J, Kakuta S, Oliva Trejo J A and Uchiyama Y 2020 Two-color in-resin CLEM of Epon-embedded cells using osmium resistant green and red fluorescent proteins *Sci Rep.* **10** 21871
- [237] Tanida I, Kakuta S, Oliva Trejo J A and Uchiyama Y 2020 Visualization of cytoplasmic organelles via in-resin CLEM using an osmium-resistant far-red protein *Sci Rep.* **10** 11314
- [238] Paez-Segala M G *et al* 2015 Fixation-resistant photoactivatable fluorescent proteins for CLEM *Nat. Methods* **12** 215–8
- [239] Fu Z, Peng D, Zhang M, Xue F, Zhang R, He W, Xu T and Xu P 2020 mEosEM withstands osmium staining and Epon embedding for super-resolution CLEM *Nat. Methods* **17** 55–8
- [240] Watanabe S, Punge A, Hoppeler G, Willig K I, Hobson R J, Davis M W, Hell S W and Jorgensen E M 2011 Protein localization in electron micrographs using fluorescence nanoscopy *Nat. Methods* **8** 80–U117
- [241] Liu B *et al* 2015 Three-dimensional super-resolution protein localization correlated with vitrified cellular context *Sci Rep.* **5** 13017
- [242] Moser F, Prazak V, Mordhorst V, Andrade D M, Baker L A, Hagen C, Grunewald K and Kaufmann R 2019 Cryo-SOFI enabling low-dose super-resolution correlative light and electron cryo-microscopy *Proc. Natl. Acad. Sci. U S A* **116** 4804–9
- [243] Chang Y W, Chen S, Tocheva E I, Treuner-Lange A, Lobach S, Sogaard-Andersen L and Jensen G J 2014 Correlated cryogenic photoactivated localization microscopy and cryo-electron tomography *Nat. Methods* **11** 737–9
- [244] Kaufmann R, Schellenberger P, Seiradake E, Dobbie I M, Jones E Y, Davis I, Hagen C and Grunewald K 2014 Super-Resolution Microscopy Using Standard Fluorescent Proteins in Intact Cells under Cryo-Conditions *Nano Lett.* **14** 4171–5
- [245] Drobizhev M, Molina R S and Franklin J 2022 Multiphoton bleaching of red fluorescent proteins and the ways to reduce it *Int. J. Mol. Sci.* **23** 770
- [246] Adhikari D P, Biener G, Stoneman M R, Badu D N, Paprocki J D, Eis A, Park P S H, Popa I and Raicu V 2021 Comparative photophysical properties of some widely used fluorescent proteins under two-photon excitation conditions *Spectrochim. Acta A Mol. Biomol. Spectrosc.* **262** 120133
- [247] Ivanchenko S, Glaschick S, Röcker C, Oswald F, Wiedenmann J and Nienhaus G U 2007 Two-photon excitation and photoconversion of EosFP in dual-color 4Pi confocal microscopy *Biophys. J.* **92** 4451–7
- [248] Drobizhev M, Makarov N S, Tillo S E, Hughes T E and Rebane A 2011 Two-photon absorption properties of fluorescent proteins *Nat. Methods* **8** 393–9
- [249] Drobizhev M, Tillo S, Makarov N S, Hughes T E and Rebane A 2009 Absolute two-photon absorption spectra and two-photon brightness of orange and red fluorescent proteins *J. Phys. Chem. B* **113** 855–9
- [250] Anzalone A V, Koblan L W and Liu D R 2020 Genome editing with CRISPR–Cas nucleases, base editors, transposases and prime editors *Nat. Biotechnol.* **38** 824–44
- [251] Eckert A F, Gao P, Wesslowski J, Wang X, Rath J, Nienhaus K, Davidson G and Nienhaus G U 2020 Measuring ligand-cell surface receptor affinities with axial line-scanning fluorescence correlation spectroscopy *eLife* **9** e55286
- [252] Wirth R, Gao P, Nienhaus G U, Sunbul M and Jäschke A 2019 SiRA: a silicon rhodamine-binding aptamer for live-cell super-resolution rna imaging *J. Am. Chem. Soc.* **141** 7562–71
- [253] Tomosugi W, Matsuda T, Tani T, Nemoto T, Kotera I, Saito K, Horikawa K and Nagai T 2009 An ultramarine fluorescent protein with increased photostability and pH insensitivity *Nat. Methods* **6** 351–3
- [254] Subach O M, Cranfill P J, Davidson M W and Verkhusha V V 2011 An enhanced monomeric blue fluorescent protein with the high chemical stability of the chromophore *PLoS One* **6** e28674
- [255] Markwardt M L *et al* 2011 An Improved cerulean fluorescent protein with enhanced brightness and reduced reversible photoswitching *PLoS One* **6** e17896
- [256] Shaner N C *et al* 2013 A bright monomeric green fluorescent protein derived from Branchiostoma lanceolatum *Nat. Methods* **10** 407–9
- [257] Bajar B T, Wang E S, Lam A J, Kim B B, Jacobs C L, Howe E S, Davidson M W, Lin M Z and Chu J 2016 Improving brightness and photostability of green and red fluorescent proteins for live cell imaging and FRET reporting *Sci Rep.* **6** 20889
- [258] Kremers G J, Goedhart J, van Munster E B and Gadella T W Jr 2006 Cyan and yellow super fluorescent proteins with improved brightness, protein folding, and FRET Förster radius *Biochemistry* **45** 6570–80
- [259] Shaner N C, Campbell R E, Steinbach P A, Giepmans B N, Palmer A E and Tsien R Y 2004 Improved monomeric red, orange and yellow fluorescent proteins derived from *Drosophila* sp. red fluorescent protein *Nat. Biotechnol.* **22** 1567–72
- [260] Chu J *et al* 2014 Non-invasive intravital imaging of cellular differentiation with a bright red-excitable fluorescent protein *Nat. Methods* **11** 572–8
- [261] Moeyaert B, Nguyen Bich N, De Zitter E, Rocha S, Clays K, Mizuno H, van Meervelt L, Hofkens J and Dedecker P 2014 Green-to-red photoconvertible dronpa mutant for multimodal super-resolution fluorescence microscopy *ACS Nano* **8** 1664–73
- [262] Andresen M, Stiel A C, Fölling J, Wenzel D, Schönle A, Egner A, Eggeling C, Hell S W and Jakobs S 2008 Photoswitchable fluorescent proteins enable monochromatic multilabel imaging and dual color fluorescence nanoscopy *Nat. Biotechnol.* **26** 1035–40
- [263] Tiwari D K, Arai Y, Yamanaka M, Matsuda T, Agetsuma M, Nakano M, Fujita K and Nagai T 2015 A fast- and positively photoswitchable fluorescent protein for ultralow-laser-power RESOLFT nanoscopy *Nat. Methods* **12** 515–8
- [264] Grotjohann T *et al* 2011 Diffraction-unlimited all-optical imaging and writing with a photochromic GFP *Nature* **478** 204–8
- [265] Pletnev S, Subach F V, Dauter Z, Wlodawer A and Verkhusha V V 2012 A structural basis for reversible photoswitching of absorbance spectra in red fluorescent protein rsTagRFP *J. Mol. Biol.* **417** 144–51
- [266] Subach F V, Patterson G H, Renz M, Lippincott-Schwartz J and Verkhusha V V 2010 Bright monomeric photoactivatable red fluorescent protein for two-color super-resolution sptPALM of live cells *J. Am. Chem. Soc.* **132** 6481–91
- [267] Subach F V, Patterson G H, Manley S, Gillette J M, Lippincott-Schwartz J and Verkhusha V V 2009 Photoactivatable mCherry for high-resolution two-color fluorescence microscopy *Nat. Methods* **6** 153–9
- [268] Gunewardene M S, Subach F V, Gould T J, Penoncello G P, Gudheti M V, Verkhusha V V and Hess S T 2011 Superresolution imaging of multiple fluorescent proteins with highly overlapping emission spectra in living cells *Biophys. J.* **101** 1522–8
- [269] Shcherbakova D M, Cox Cammer N, Huisman T M, Verkhusha V V and Hodgson L 2018 Direct multiplex imaging and optogenetics of Rho GTPases enabled by near-infrared FRET *Nat. Chem. Biol.* **14** 591–600
- [270] Yu D *et al* 2015 A naturally monomeric infrared fluorescent protein for protein labeling *in vivo* *Nat. Methods* **12** 763–5